JAN 09 1998

0830 L-02 NAS1.29/3-2:98-01

NASA Tech Briefs

National Aeronautics and
Space Administration

Electronic Components and Circuits

Electronic Systems

Physical Sciences

Materials

Computer Programs

Mechanics

Machinery

Fabrication Technology

Mathematics and Information Sciences

Life Sciences

1999-035336

98-01

January 1998

INTRODUCTION

Tech Briefs are short announcements of new technology derived from the research and development activities of the National Aeronautics and Space Administration. These Briefs emphasize information considered likely to be transferable across industrial, regional, or disciplinary lines and are issued to encourage commercial application.

Availability of NASA Tech Briefs and TSP's

Distribution of NASA Tech Briefs, a monthly periodical publication, is limited to engineers in U.S. Industry and to other domestic technology transfer agents. Requests for individual Tech Briefs or for Technical Support Packages (TSP's) announced herein should be addressed to

NASA Center for AeroSpace Information
Technology Transfer Office
800 Elkridge Landing Rd.
Linthicum Heights, MD 21090-2934
Telephone No. (301) 621-0245

Please reference the three-letter, five-digit control number located at the end of each Tech Brief. Information on NASA's Technology Utilization Program, its documents, and services is also available at the same facility.

Technology Utilization Officers and Patent Counsels are located at NASA field installations to provide technology-transfer access to industrial users. Inquiries can be made by writing to NASA field installations listed below.

Technology Utilization Officers and Patent Counsels

Ames Research Center
Technology Utilization Officer
Mail Code 223-3
Moffett Field, CA 94035

Patent Counsel
Mail Code 200-11
Moffett Field, CA 94035

Goddard Space Flight Center
Technology Utilization Officer
Mail Code 702-1
Greenbelt, MD 20771

Patent Counsel
Mail Code 204
Greenbelt, MD 20771

Lyndon B. Johnson Space Center
Technology Utilization Officer
Mail Code IC-4
Houston, TX 77058

Patent Counsel
Mail Code AL3
Houston, TX 77058

John F. Kennedy Space Center
Technology Utilization Officer
Mail Stop PT-PMO-A
Kennedy Space Center, FL 32899

Patent Counsel
Mail Code PT-PAT
Kennedy Space Center, FL 32899

Langley Research Center
Technology Utilization Officer
Mail Stop 143
Hampton, VA 23665

Patent Counsel
Mail Code 279
Hampton, VA 23665

Lewis Research Center
Technology Utilization Officer
Mail Stop 7-3
21000 Brookpark Road
Cleveland, OH 44135

Patent Counsel
Mail Code LE-LAW
21000 Brookpark Road
Cleveland, OH 44135

Jet Propulsion Laboratory
Technology Utilization Officer
Mail Stop 156-211
4800 Oak Grove Drive
Pasadena, CA 91109

NASA Resident Office-JPL
Technology Utilization Officer
Mail Stop 180-801
4800 Oak Grove Drive
Pasadena, CA 91109

Patent Counsel
Mail Code 180-801
4800 Oak Grove Drive
Pasadena, CA 91109

George C. Marshall Space Flight Center
Technology Utilization Officer
Code AT01
Marshall Space Flight Center, AL 35812

Patent Counsel
Mail Code CC01
Marshall Space Flight Center, AL 35812

John C. Stennis Space Center
Technology Utilization Officer
Code HA-30
Stennis Space Center, MS 39529

NASA Headquarters
Technology Utilization Officer
Code CU
Washington, DC 20546

Assistant General Counsel for Patent Matters
Code GP
Washington, DC 20546

Dryden Flight Research Center
Technology Utilization Officer
M/S D21-31
Bldg. 4832 Whse 7
Lilly Dr.
Edwards, CA 93523

NASA TechBriefs

National Aeronautics and Space Administration

January 1998
98-01

5 Electronic Components and Circuits

13 Electronic Systems

17 Physical Sciences

23 Materials

27 Computer Programs

31 Mechanics

37 Fabrication Technology

41 Mathematics and Information Sciences

45 Life Sciences

This document was prepared under the sponsorship of the National Aeronautics and Space Administration. Neither the United States Government nor any person acting on behalf of the United States Government assumes any liability resulting from the use of the information contained in this document, or warrants that such use will be free from privately owned rights.

BLANK PAGE

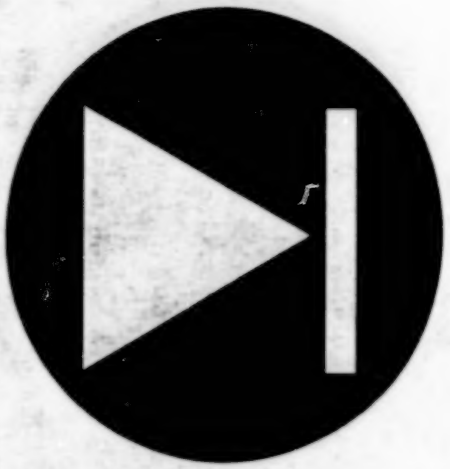

Electronic Components and Circuits

Hardware, Techniques, and Processes

7 Signal-Conditioning Electronics for Discrete Capacitive Sensors
7 Polyimide Passivation for Making High-T_c Josephson Junctions
8 Phase-Synchronized Enhancement Method for Engine Diagnostics
9 Cross-Grating Coupling for Focal-Plane Arrays of QWIPs
10 Two-Wavelength Focal-Plane Array of QWIPs
11 Reducing Surface Leakage Currents in FPAs of QWIPs

BLANK PAGE

Signal-Conditioning Electronics for Discrete Capacitive Sensors

The effects of stray capacitance are nullified with a parallel resonant circuit.

Marshall Space Flight Center, Alabama

A newly developed instrument, designed at Marshall Space Flight Center, uses the resistance to alternating current running through a device to measure the variances in capacitance. Engineers use this device to detect the presence or absence of dielectric material between the plates of a capacitor.

Previously, instruments were designed to measure one or more quantities (amplitude, frequency, or phase) that make up an alternating current waveform. However, these instruments were plagued by stray capacitance, solder traces and connectors.

This device allows engineers to apply Ohm's law to make an impedance measurement of the sensor by knowing the voltage across the sensor and the current running through the sensor.

An inductive circuit is in parallel with the stray capacitance from the sensor cable, connectors, and solder traces on the printed circuit board within this device. This unique design puts the inductor and stray capacitance [including the cable capacitance at the end of a 300- to 400-ft (90- to 120-m) cable] in a parallel resonant circuit that completely nullifies the effects of stray capacitance. Because stray capacitances no longer have any affect on the measurement system, the circuit is said to be tune.

The signal conditioning electronics for this instrument are shown in the abbreviated schematic diagram below. The sensor is excited by a 1-V (rms) sine wave that is operated at 10 kHz. The signal is then sent through a coaxial cable to the capacitive sensor. (The coaxial cable shields the signal from any outside disturbance.) The signal at the sensor is again picked off from another coaxial cable to the right of the sensor and sent to the instrument in a series across the resistor. The current sense resistor prevents the current flow across the sensor from loading down the signal. The resulting signal is then fed to an amplifier.

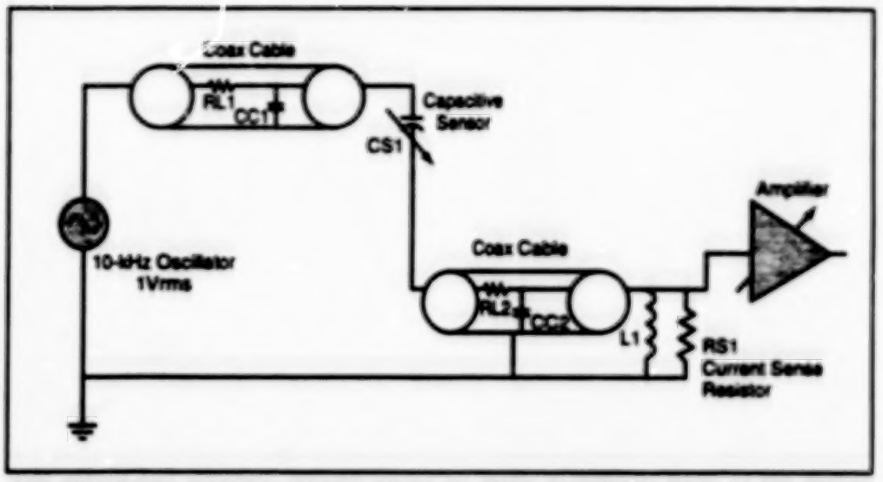

This abbreviated schematic diagram shows the Major Functional Parts of the Signal-Conditioning Electronics for discrete capacitive sensors.

The amplified signal is fed to a comparator circuit. If the voltage on the non-inverting terminal of the comparator exceeds the trip voltage setting on the inverting terminal, the output of the comparator goes high, turning the transistor ON, indicating that the capacitive plates are covered by the dielectric material. An OFF transistor reading indicates the sensor is no longer exposed to the dielectric material.

This work was done by Randal S. McNichol of the **Marshall Space Flight Center.** *Further information is contained in a TSP [see page 1].*
MFS-31195

Polyimide Passivation for Making High-T_c Josephson Junctions

Smaller spreads in critical currents and resistances are achieved.

NASA's Jet Propulsion Laboratory, Pasadena, California

Passivation by coating with OCG285 (or equivalent) polyimide at critical steps of fabrication has been found to enhance the quality of tapered edges in high-critical-temperature (high-T_c) superconductor/-normal-conductor/superconductor (SNS) Josephson junctions. In comparison with Josephson junctions that are nominally identical except for having been fabricated without such passivation, those fabricated with polyimide passivation exhibit cleaner and smoother edges and, consequently, smaller differences among the resistances and critical currents of individual junctions.

The formation of clean, smooth, tapered edges on films of high-T_c superconductors (primarily $YBa_2Cu_3O_{7-\delta}$) and on related epitaxial insulating films (e.g., $SrTiO_3$) is an essential part of the fabrication of SNS Josephson junctions and similar devices. The tapered edges are needed for the subsequent deposition of layers that are free of defects. In typical current practice, the edges are formed by ion milling through photoresist masks that have been patterned onto the high-T_c superconducting and overlying insulating films. This processing exposes the superconducting films to the photoresist patterning, which often leaves minute amounts of residues that degrade the quality of subsequently deposited high-T_c superconducting films. In addition, the exposure of the photoresist and superconducting films to the ion-milling process can lead to further degradation of the superconductor films and edges.

Figure 1 shows one aspect of the formation of a tapered edge in a process that incorporates the polyimide passivation step. Coating with the polyimide before patterning and ion milling protects the underlying high-temperature superconductor from the developer and photoresist. The polyimide layer also protects the photoresist against ion-milling-induced changes that degrade the superconducting film and edges.

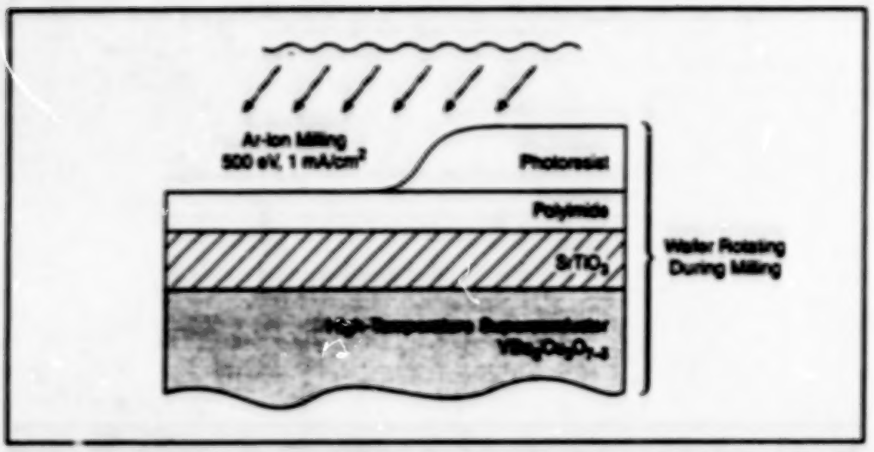

Figure 1. The Formation of a Tapered Edge on a high-temperature superconductor during the fabrication of an SNS Josephson junction is accomplished by ion milling through a patterned photoresist mask. The incorporation of the polyimide layer enhances the quality of the tapered edge formed in this process.

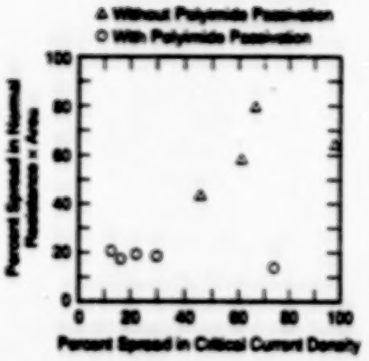

Figure 2 The Spreads in Resistance and Critical Current for sample SNS Josephson junctions fabricated without and with polyimide were calculated from current-vs.-voltage measurements. The percent spread on each axis is defined as 100 × (the standard deviation ÷ the mean).

The polyimide-passivation technique has been tested in the fabrication of multiple SNS edge Josephson junctions on chips. $YBa_2Cu_3O_{7-\delta}$ followed by $SrTiO_3$ was deposited on (100) $LaAlO_3$ wafers. The $SrTiO_3$ layers were patterned with reflowed photoresist masks, then rotated during argon-ion milling without cooling. The Josephson junctions were then completed by the deposition of $YBa_2Cu_{2.79}Co_{0.21}O_{7-\delta}$ as the normal conductor followed by $YLa_{0.008}Ba_2Cu_3O_{7-\delta}$ superconducting counterelectrodes. The current-vs.-voltage characteristics of junctions fabricated with and without polyimide passivation were measured at a temperature of 60 K. Plotted in Figure 2 are the spreads in the critical current densities and quantities proportional to normal resistivities calculated from the measurements. The results show that in all cases except one, the variability among devices was decreased by use of polyimide passivation. In the one exceptional case in which a chip made with polyimide passivation exhibited a 74-percent spread in critical current, the SNS devices on the chip were just beginning to show a critical current as the temperature decreased to the measurement temperature; at a temperature of 50 K, the spread in critical current for this chip was 24 percent.

This work was done by Jeffrey Barner and Henry LeDuc of Caltech for **NASA's Jet Propulsion Laboratory**. *Further information is contained in a TSP [see page 1].*
NPO-20164

Phase-Synchronized Enhancement Method for Engine Diagnostics

This technique transforms instantaneous phase signals into discrete signals for better engine-health monitoring and fault analysis.

Marshall Space Flight Center, Alabama

A diagnostic signal-analysis technique, called the Phase Synchronized Enhancement Method (PSEM), has been developed. This method allows NASA engineers to retrieve any unique defect signatures and trends associated with different failure modes and unusual phenomena experienced during Space Shuttle main engine (SSME) testing.

Previous diagnostic studies using the Generalized Hyper-Coherence method have shown that the frequency of the shaft rotational component (sync) of a high-speed SSME turbopump is fluctuating around a center frequency during steady-state operation. These studies further showed the Power Spectral Density (PSD) to be exhibiting a discrete peak, indicative of strong stationarity.

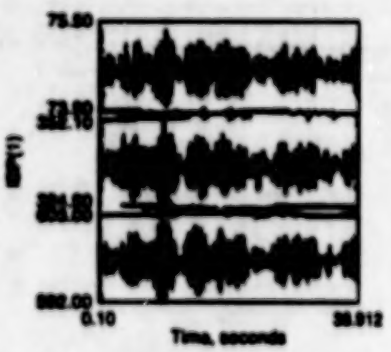

This illustration shows the Instantaneous Frequency of sync (N), inner ball pass (IBP), and the 8th harmonic of sync (8N). PSEM algorithm forces the frequency of sync from this periodic variation into a constant frequency, generating a highly desirable effect on the entire signal.

Machinery failure detection has always been a significant technical challenge for NASA's propulsion technology engineers. A reliable engine-health-monitoring system can prevent catastrophic failures and lower costly downtime due to false alarms. PSEM can provide valuable signal-enhancement capability during engine-health monitoring and diagnostics and improve the safety and reliability of NASA's advanced propulsion systems.

This method of analysis uses the microfrequency variation phenomenon to improve all the sync-related components in a signal. PSEM forces the narrow-band spectral component of sync into a pure-tone discrete component with a constant frequency by transforming its instantaneous phase signal into an equivalent

"realignment" time. When the realignment time is corrected, the original sync component will become discrete, generating a highly desirable effect on the entire signal where all the other sync-related components (sync harmonics, cage, ball spin, outer ball pass, and inner ball pass) will automatically become discrete. The resulting discrete signal provides better PSD resolution, which improves engine diagnostic evaluation.

A vibration signal in a rotor system is modeled as an FM signal with multiple spectral components at different carrier frequencies. The instantaneous frequency and instantaneous phase information of each component is recovered using several digital frequency-demodulation methods, such as complex demodulation techniques and the phase-lock-loop method. During steady-state operation of most machinery systems, the instantaneous frequency of sync tends to fluctuate about a center frequency and is not a constant frequency. Since the amplitude of such frequency variation could be much smaller than the bandwidth with PSD analysis, the sync spectral component still appears as a very discrete peak in its PSD.

This technique has potential for commercial application outside NASA's propulsion area. For example, PSEM will greatly increase the PSD resolution during quality-control checks on spindle motors during production and reduce the man-hours needed for system monitoring and diagnostics.

This work was done by Jen-Yi Jong of AI Signal Research, Inc., for the **Marshall Space Flight Center**. *Further information is contained in a TSP [see page 1].*
MFS-26435

Cross-Grating Coupling for Focal-Plane Arrays of QWIPs

Narrow-band coupling with increased efficiency could be achieved.

NASA's Jet Propulsion Laboratory, Pasadena, California

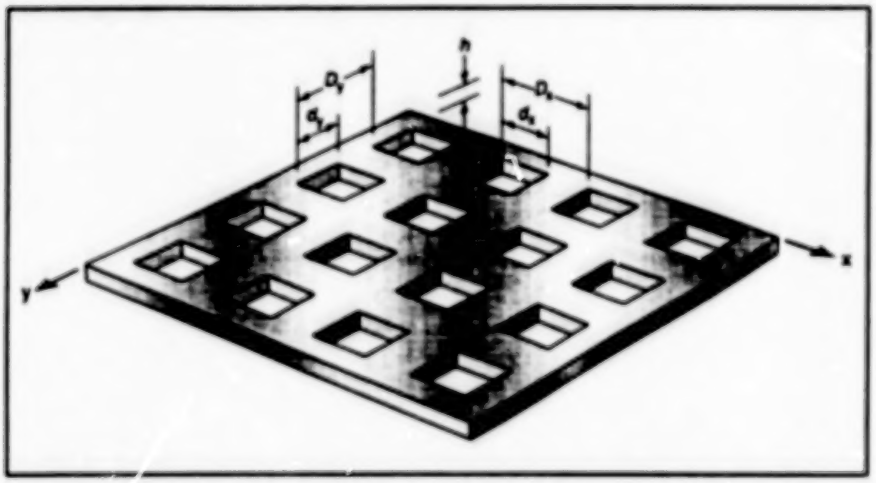

Figure 1. A Diffraction Grating containing a rectangular planar array of holes would provide wavelength-selective coupling to an adjacent focal-plane array of QWIPs.

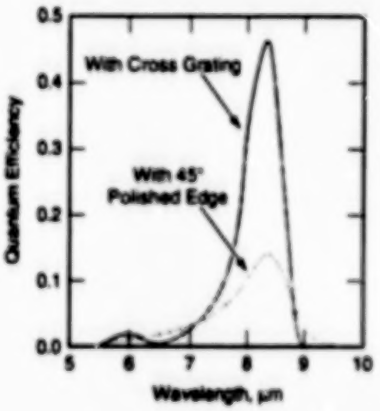

Figure 2. Quantum Efficiency and Wavelength Selectivity would be increased by use of an optimized cross grating instead of a 45°-polished-edge reflector.

Cross-diffraction gratings have been proposed to provide optical coupling to quantum-well infrared photodetectors (QWIPs) in focal-plane arrays (FPAs). The cross-grating coupling scheme is intended to enhance optical coupling (and thus increase quantum efficiency) within narrow spectral bands; this would make it possible to construct improved wavelength-selective infrared-imaging instruments for a variety of scientific, industrial, and military applications.

The structure of a QWIP FPA poses an optical-coupling problem because of a confluence of three considerations:

1. The direction through the thicknesses of the quantum wells is perpendicular to the focal plane;
2. Quantum selection rules allow the detection of only that part of the incident light that is electrically polarized along the direction through the thicknesses of the quantum wells and thus perpendicular to the focal plane; and
3. The light to be detected is incident along directions approximately perpendicular to the focal plane, and thus only a small fraction of it is electrically polarized along the thicknesses of the quantum wells.

Heretofore, the coupling problem has been solved by use of random reflectors, which provide reasonable coupling efficiency over a broad spectral band. Like random reflectors, crossed diffraction gratings would effect the desired conversion of polarization via scattering; however, the inherent periodicity of a diffraction grating could be exploited to enhance conversion at a desired wavelength. The design of a cross grating for this purpose involves the following mathematical model (see Figure 1): The grating is considered to be a perfectly electrically conductive slab with a rectangular array of holes through its thickness, and each hole is regarded as a waveguidelike cavity. The task is to choose the dimensions of the grating to maximize the power diffracted, at the desired wavelength, from a normally incident beam into waveguide modes with through-the-thickness polarization.

In a preliminary assessment of the utility of the cross-grating concept, the absorption quantum efficiency as a function of wavelength was computed for a QWIP FPA of 30-by-30-μm pixels with a cross grating optimized for a wavelength of 8.4 μm and light incident through *f*/2.3 optics. The result of this computation was compared with the measured quantum efficiency vs. wavelength of the same QWIP with a 45°-polished-edge reflector instead of a cross grating. As illustrated in Figure 2, the computation predicted that the use of the cross grating would increase the

quantum efficiency at the wavelength of 8.4 μm wavelength and would reduce the width of the spectral pass band.

This work was done by Sarath D. Gunapala and Sumith V. Bandara of Caltech for **NASA's Jet Propulsion Laboratory**. *Further information is contained in a TSP [see page 1].*

In accordance with Public Law 96-517, the contractor has elected to retain title to this invention. Inquiries concerning rights for its commercial use should be addressed to

Technology Reporting Office
JPL
Mail Stop 122-116
4800 Oak Grove Drive
Pasadena, CA 91109
(818) 354-2240

Refer to NPO-19657, volume and number of this NASA Tech Briefs *issue, and the page number.*

Two-Wavelength Focal-Plane Array of QWIPs

One device could image the same scene at two wavelengths simultaneously.

NASA's Jet Propulsion Laboratory, Pasadena, California

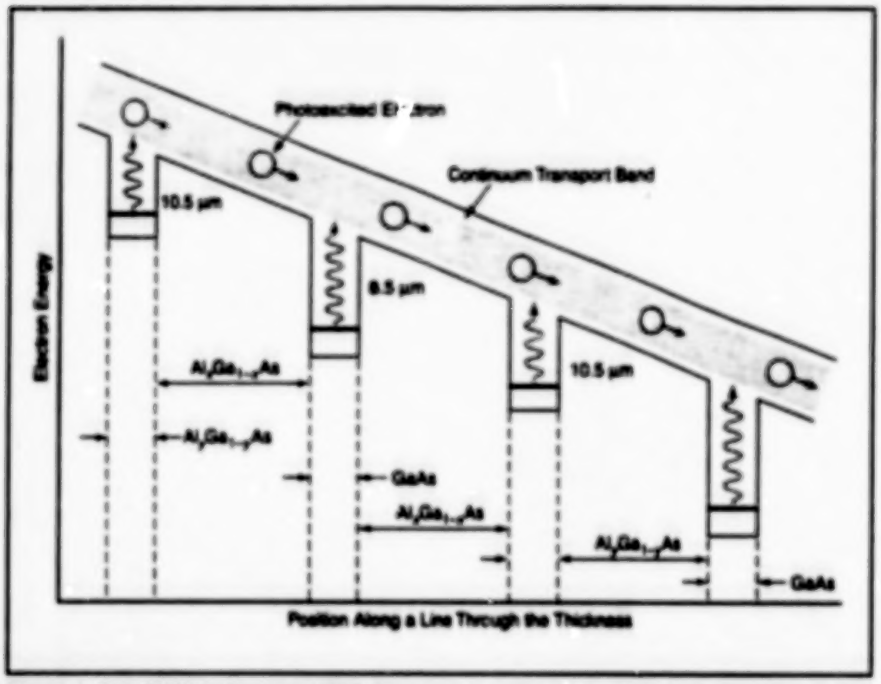

Figure 1. The Multiple-Quantum-Well Structure is designed to obtain peak response at two wavelengths and to provide a smooth continuum transport band (to prevent quantum reflections at the barriers).

A proposed focal-plane array (FPA) of quantum-well infrared photodetectors (QWIPs) would exhibit peak response at two wavelengths. Heretofore, single-focal-plane arrays of photodetectors optimized for two or more wavelengths have not been available. This FPA is intended to be a prototype of multispectral imaging devices for a variety of scientific, industrial, and military infrared instruments.

In the proposed device, the two-wavelength-peak response would be achieved by use of a multiple-alternating-quantum-well structure in $Al_xGa_{1-x}As$ photodetectors (see Figure 1). This structure would comprise 50 periods of alternating quantum wells. The energy depth and geometric thickness of the first well in each period would be optimized to obtain peak response at a wavelength of 8.5 μm; the corresponding parameters of the second well in each period would be optimized for peak response at a wavelength of 10.5 μm. The quantum wells would be separated by $Al_xGa_{1-x}As$ barriers 500 Å thick.

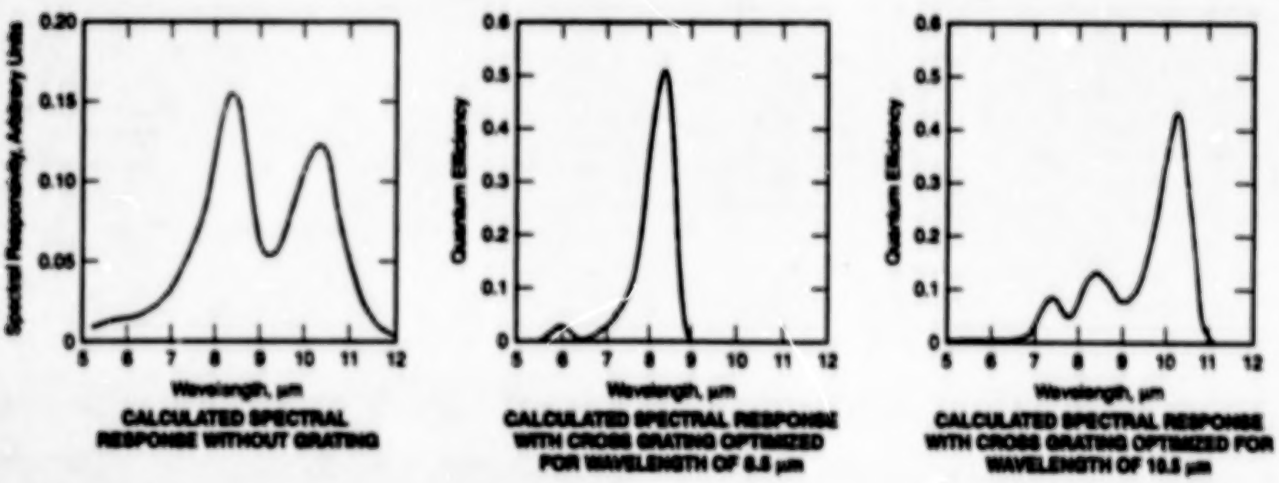
Spectral Responsivity, Arbitrary Units
Wavelength, μm
CALCULATED SPECTRAL RESPONSE WITHOUT GRATING
Quantum Efficiency
Wavelength, μm
CALCULATED SPECTRAL RESPONSE WITH CROSS GRATING OPTIMIZED FOR WAVELENGTH OF 8.5 μm
Quantum Efficiency
Wavelength, μm
CALCULATED SPECTRAL RESPONSE WITH CROSS GRATING OPTIMIZED FOR WAVELENGTH OF 10.5 μm

Figure 2. The Two-Peak Spectral Response of the proposed QWIP could be changed to single-peak responses by cross diffraction gratings.

To prevent additional quantum reflections in the continuum transport band at the locations of the barriers, all the barriers would have to be of the same energy height and thus fabricated with the same proportion (x) of aluminum. The wells for 8.5-μm peak response would be made of GaAs. The wells for 10.5-μm response, being of a different energy depth, would have to be made with a different proportion (y) of aluminum.

The top part of Figure 2 shows the calculated spectral responsivity of the proposed QWIP. To increase quantum efficiency and wavelength selectivity, the FPA would also include cross diffraction gratings like those described in the companion article, "Cross-Grating Coupling for Focal-Plane Arrays of QWIPs" (NPO-19657). These gratings would be optimized for the wavelengths of 8.5 and 10.5 μm and would be positioned in alternation over successive columns. As a result, all the photodetectors in one column would exhibit peak response at one of these wavelengths and all the photodetectors in the next column would exhibit peak response at the other wavelength, as shown in the lower part of Figure 2. Thus, the FPA would detect two column-interlaced images of the same scene in different wavelength bands. The outputs from the photodetectors in alternate columns could be fed to two video monitors to display both wavelength images simultaneously.

This work was done by Sarath D. Gunapala, Sumith V. Bandara, True L. Lin, and Jin S. Park of Caltech for **NASA's Jet Propulsion Laboratory**. *Further information is contained in a TSP [see page 1].*

In accordance with Public Law 96-517, the contractor has elected to retain title to this invention. Inquiries concerning rights for its commercial use should be addressed to

Technology Reporting Office
JPL
Mail Stop 122-116
4800 Oak Grove Drive
Pasadena, CA 91109
(818) 354-2240

Refer to NPO-19658, volume and number of this NASA Tech Briefs *issue, and the page number.*

Reducing Surface Leakage Currents in FPAs of QWIPs

Total dark currents could be reduced substantially.

NASA's Jet Propulsion Laboratory, Pasadena, California

Chemical surface treatments during fabrication have been proposed to reduce surface leakage currents in focal-plane arrays (FPAs) of quantum-well infrared photodetectors (QWIPs). For reasons explained below, if most or all of the surface leakage currents could be eliminated by such treatments, then total dark currents could be reduced to about 1/4 or 1/5 of their original values.

The surface leakage current of a QWIP is a component of its dark current and is proportional to its circumference. The other components of the dark current of a QWIP originate within the bulk of its material and are proportional to its area. By fundamental geometry, the ratio between circumference and area is inversely proportional to width. Thus, as a QWIP is made narrower to incorporate it into a FPA, the ratio between its surface leakage current and the other components of its dark current increases. At the typical lateral dimensions (40 by 40 μm) of a QWIP in an FPA, the surface leakage current is about 4 times the total of all the other components of dark current; that is, the surface leakage current constitutes about 4/5 of the dark current.

Since the earliest days of solid-state electronics, it has been recognized that surfaces and interfaces play a decisive role. Solid-state electronic devices are uniquely sensitive to electrically active surface sites, even at concentrations as small as one part per million. Electrically active surface sites originate in unsatisfied covalent bonds. By satisfying all covalent surface bonds, one could shift surface electron-energy states out of the band gap and into the valence and conduction bands, thereby reducing the surface leakage current. The proposed surface chemical treatments are intended to satisfy the covalent bonds. They include treatment of open surfaces with inorganic sulfides (e.g., LiS_2, NH_4S, or $Na_2S{\cdot}9H_2O$) or using NH_4OH wet chemical etch to define mesas and passivating open areas with SiN.

This work was done by Sarath D. Gunapala, Mani Sundaram, Jin S. Park, Sumith V. Bandara, and John K. Liu of Caltech for **NASA's Jet Propulsion Laboratory**. *Further information is contained in a TSP [see page 1].*

In accordance with Public Law 96-517, the contractor has elected to retain title to this invention. Inquiries concerning rights for its commercial use should be addressed to

Technology Reporting Office
JPL
Mail Stop 122-116
4800 Oak Grove Drive
Pasadena, CA 91109
(818) 354-2240

Refer to NPO-19669, volume and number of this NASA Tech Briefs *issue, and the page number.*

BLANK PAGE

Electronic Systems

Hardware, Techniques, and Processes

15 VLSI Neural Processors Based on Optimization Neural Networks

BLANK PAGE

VLSI Neural Processors Based on Optimization Neural Networks

Computational performances could be greatly enhanced.

NASA's Jet Propulsion Laboratory, Pasadena, California

Compact analog/digital electronic data processors of a novel type are based on the concept of the optimization cellular neural network (OCNN) and are implemented in very-large-scale integrated (VLSI) circuitry. These VLSI neural processors are being developed to perform a variety of computation-intensive tasks in maximizing the return of useful scientific information from future multiple-sensor microspacecraft, given such considerations as synergy among multiple sensors, limits on the power and bandwidth available for transmission of data, and the need to recognize significant data in the absence of prior explicit instructions. The OCNN concept also has obvious potential for terrestrial "smart"-sensor and other data-reduction applications.

The OCNN concept is founded on the concept of the cellular neural network (CNN), which is a recursive neural network that comprises a multidimensional array of mainly identical artificial neural cells, wherein (1) each cell is a dynamic subsystem with continuous state variables and (2) each cell is connected to only the few other cells that lie within a specified radius (see Figure 1). Since its original publication in 1988, the concept of the CNN has evolved rapidly and now provides a unified theoretical framework for such computation-intensive applications as signal processing and optimization. The CNN concept provides the architecture for a locally connected, massively parallel computing system with simple synaptic operators — very suitable for VLSI implementation in real-time, high-speed applications. The behavior of a CNN depends on the computing model, network topology, and coefficient template; the behavior in a given application depends primarily on the coefficients of the template (synaptic weights, threshold values, and boundary conditions) and the procedure for applying them.

An OCNN is designed to perform programmable functions for fine-grained processing with annealing control to enhance the quality of the output. Going beyond the basic CNN concept, the OCNN concept incorporates a hardware-based annealing method, according to which the annealing function is embedded in the network. The annealing function is a parallel version of fast mean-field annealing in analog networks, and is highly efficient in finding globally optimal solutions. Whereas synaptic weights in a basic CNN are fixed, those in an OCNN are made digitally programmable to accommodate applications in which predetermined operators are needed.

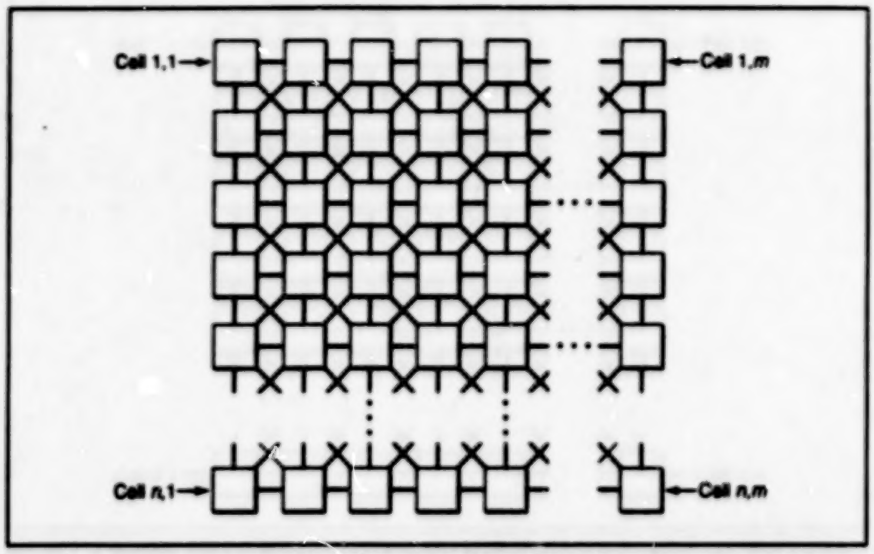

Figure 1. A Typical *n*-by-*m* Rectangular Cellular Neural Network contains cells that are connected to their nearest neighbors only.

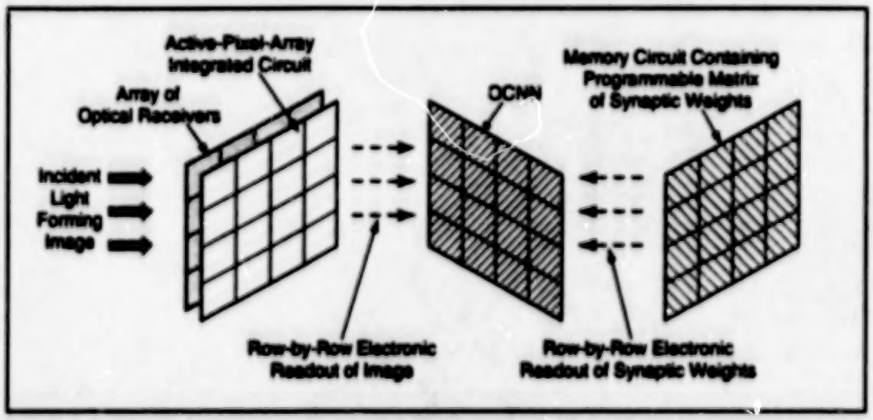
Active-Pixel-Array Integrated Circuit
Array of Optical Receivers
Incident Light Forming Image
OCNN
Memory Circuit Containing Programmable Matrix of Synaptic Weights
Row-by-Row Electronic Readout of Image
Row-by-Row Electronic Readout of Synaptic Weights

Figure 2. A "Smart" Optoelectronic Image Sensor could include an OCNN sandwiched between a planar array of optical receivers and a planar array of optical transmitters, along with circuitry that would implement a programmable synaptic-weight matrix memory. This combination of optics and electronics would afford fast processing of sensory information within the sensor package.

Other important features of the OCNN concept can be described with reference to the example of a typical intended application, in which a VLSI OCNN processor would receive input from an image-sensing array of photodetectors and would perform such image-data-processing functions as detecting edges or detecting motion. If a basic CNN were to be used in this application, then each pixel would be represented by one neuron. In an OCNN, every pixel could be represented by multiple neurons, that, collectively, would constitute a hyperneuron and would execute the maximum evolution function for selecting among various profiles or exploiting data synergy. For instance, in an OCNN designed to detect motion, every image pixel would be represented by multiple, mutually exclusive neurons in a hyperneuron for velocity selection. Only the winning neuron within each hyperneuron would remain active, while the others would be turned off. The operation of the neural network would be terminated when the energy function of the network reached a minimum. To improve the global interconnections and the input and output of image data with external circuitry beyond those of

a basic CNN, an OCNN could be integrated with optical receivers and transmitters (see Figure 2).

VLSI neural processors of this type would likely also prove useful in terrestrial robotic systems and in other systems in which there are requirements for "smart" sensor subsystems and/or high-performance on-board computing for optimization, autonomous control, and/or reduction of data. Preliminary studies have shown that the OCNN concept offers the potential for orders-of-magnitude improvements in performance in onboard computation for autonomous control and reduction of data from multiple sensors.

This work was done by Wai-Chi Fang, Bing J. Sheu, and James Wall of Caltech for **NASA's Jet Propulsion Laboratory**. *Further information is contained in a TSP [see page 1].*

In accordance with Public Law 96-517, the contractor has elected to retain title to this invention. Inquiries concerning rights for its commercial use should be addressed to

Technology Reporting Office
JPL
Mail Stop 122-116
4800 Oak Grove Drive
Pasadena, CA 91109
(818) 354-2240

Refer to NPO-19989, volume and number of this NASA Tech Briefs *issue, and the page number.*

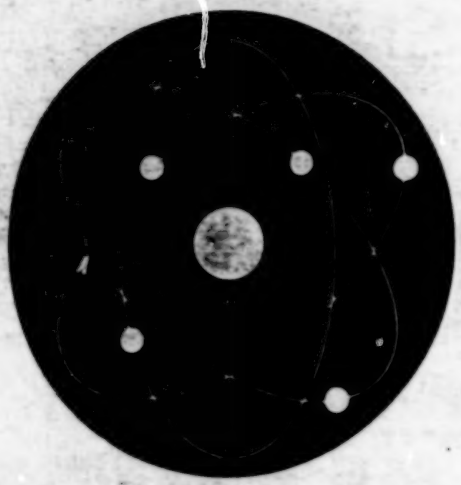

Physical Sciences

Hardware, Techniques, and Processes

19 Black-Body Evaporator Unit for a Point-Focus Solar Collector
20 Integrated Thin-Film Fluorescence Sensor
20 Calculating Chemical-Reaction Rates From Thermodynamic Data
21 Proximity Measurement of Pressure and Temperature
22 Adjacent-Pair Imaging Shearography Using Bacteriorhodopsin

Books and Reports

22 Potential Commercial Applications From Microgravity Combustion Research

BLANK PAGE

Black-Body Evaporator Unit for a Point-Focus Solar Collector

A special coating is not necessary to ensure high solar absorptivity.

John F. Kennedy Space Center, Florida

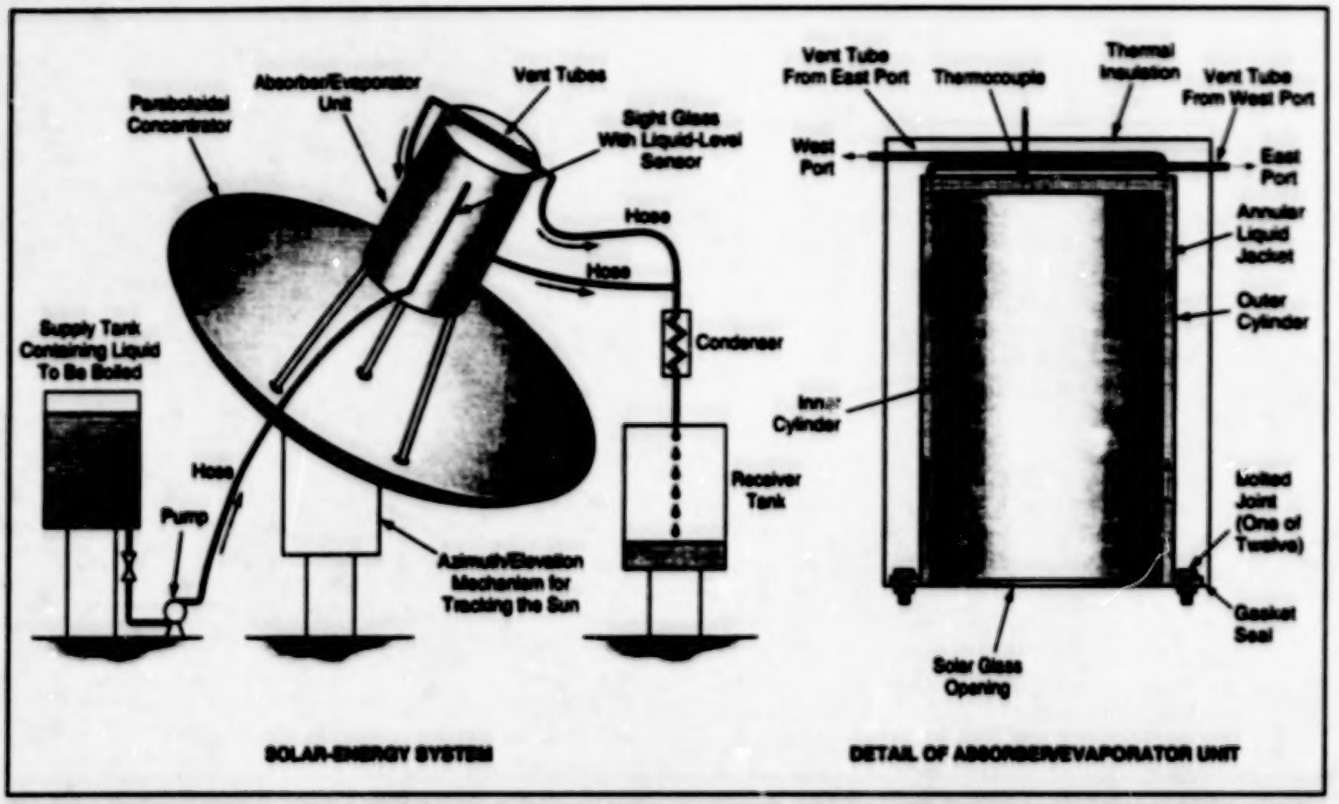

The Solar Heating System for boiling a liquid features an improved absorber/evaporator unit that exploits geometry to achieve an absorption characteristic approximating that of a black body. The seemingly peculiar arrangement of vent tubes can be understood, upon closer examination, to prevent spillage of liquid when the unit is tilted toward the east or west.

The figure illustrates a solar thermal energy system for boiling water or another liquid. The system can be used for a variety of purposes that can include drying aqueous hazardous waste, distilling pure solvent from spent solvent, purifying water by distillation, or generating steam. The principal innovative feature of this system is an absorber/evaporator unit, which is designed to absorb radiant solar energy with an effectiveness close to that of an ideal (in the black-body sense) absorber. The design is such that unlike in some other systems, it is not necessary to coat the solar-irradiated surface with a high-solar-absorptivity ("solar black") material to obtain the desired black-body characteristic. The design is also simpler than that of other absorber/evaporator units.

Though the absorber/evaporator unit described here is cylindrical, it could just as well have a spherical, conical, or other convenient shape. The absorber/evaporator unit includes an inner cylinder and a slightly wider outer cylinder, both made of stainless-steel sheet. The inner cylinder acts as the solar-energy absorber for heating the liquid, which is pumped into the narrow annulus between the inner and outer cylinders. The narrow-annulus feature is an important element of the design in that a liquid can be boiled most effectively when confined in a thin layer. The vapor leaves through vent tubes at the top, then flows through vent hoses to the condenser. The vent tubes, the vent hoses, and the outer surface of absorber/evaporator unit (except at the opening) are covered with insulating material.

Concentrated solar radiation enters the absorber/evaporator unit through a solar-glass-covered opening at its lower end. The absorber/evaporator unit is positioned and oriented to face a paraboloidal solar-radiation concentrator; the cylindrical axis of the unit is aligned with the optical axis of the concentrator and the unit is positioned along this axis with the center of the opening at the focal point of the concentrator. Of course, the paraboloidal concentrator must be mounted on an azimuth/elevation tracking mechanism that keeps the concentrator aimed toward the Sun.

This optical arrangement ensures that most or all of the concentrated solar radiation enters the cavity enclosed by the inner cylinder, yet the opening is small enough to provide a relatively small solid angle for the escape of thermal radiation from the cavity. Once solar radiation enters the cavity, some is absorbed immediately, some is absorbed after one or more reflection(s), some is reradiated, and some of the reflected and reradiated energy escapes through the opening. The opening is small enough that the solid angle for the escape of radiation is relatively small; consequently, the incident radiation undergoes multiple cycles of reflection, absorption, and reradiation that convert the radiation field in the cavity into one that approximates a black-body radiation field, even in the absence of a high-absorptivity coating on the absorber surface.

With its thin-wall-shell design and without a special high-absorptivity coating, the absorber/evaporator unit can be constructed relatively easily. The unit can also be disassembled relatively easily for cleaning and repair.

This work was done by Feng-Nan Lin, William I. Moore, and Philip D. Strode of **Kennedy Space Center.** *Further information is contained in a TSP [see page 1].*
KSC-11895

Integrated Thin-Film Fluorescence Sensor

This device senses fluorescence at a wavelength characteristic of a substance to be detected.

Lewis Research Center, Cleveland, Ohio

An integrated thin-film device has been designed to constitute the sensory element of a miniature instrument for measuring the concentration of an atomic or molecular species that exhibits fluorescence at specified excitation and emission wavelengths. The device combines a fluorescence-emission method with a diffraction method to detect fluorescence emitted by those atoms or molecules of interest that are situated within a short distance of one surface of the device. Applications could be as diverse as medical and biological immunoassay and monitoring pollutant gases in engine exhausts.

The device comprises multiple corrugated thin film layers (see figure). The corrugations are characterized by a peak-to-valley depth of about 500 Å and a spatial period of about 1 μm. The function of the corrugations is explained below.

The layer in contact with the atmosphere or other medium that contains the fluorescent material to be detected is a dielectric waveguide with a thickness of the order of 2,000 Å. The thickness is chosen so that the waveguide supports the desired electromagnetic-field modes at the specified fluorescence excitation and emission wavelengths. The electric-field profiles of these modes are evanescent; that is, outside the waveguide layer, the electric-field amplitudes decrease monotonically with distance from the layer.

Optical excitation is supplied by radiation from an external source to fluorescent atoms or molecules near the surface. The resulting emission from the fluorescent atoms or molecules is coupled into the waveguide via evanescent wave modes; thus, the device opens a radiative-decay channel for fluorescence.

Below the dielectric waveguide is a metal film. Below the metal film is a dielectric buffer layer made of a material different from that of the waveguide layer. Among the electromagnetic-field modes supported by the thin-film geometry are surface plasmons, supported at the dielectric/metal interface. The amplitudes of these modes decay with increasing depth into the metal. The thickness of the metal layer is about 500 Å — enough to render the metal opaque to photons but not enough to prevent overlap of plasmon fields on opposite surfaces.

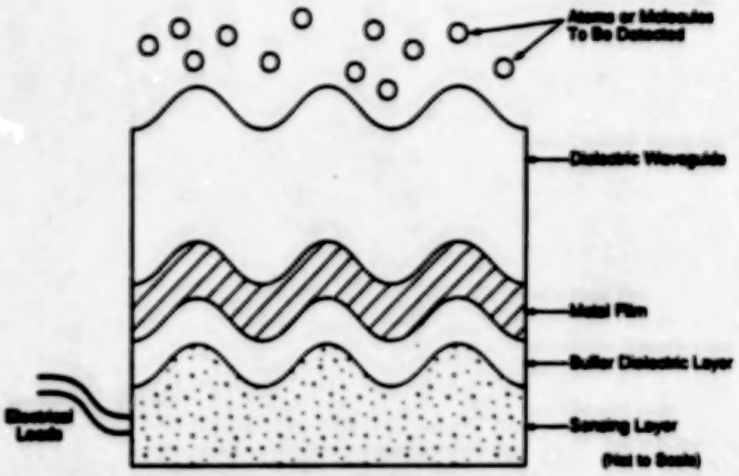

The Corrugated Dielectric and Metal Layers of this device are designed to exploit evanescent-wave coupling and cross-coupling of surface plasmons so that fluorescent emission from nearby atoms or molecules to be detected is coupled to the sensing layer, while light at other wavelengths is not coupled to the sensing layer.

In this asymmetric dielectric/metal/dielectric configuration, the corrugation enables matching of the momenta of surface plasmons that have equal wavelength and are localized on opposite sides of the metal film. As a result, over a narrow range of wavelengths, there is cross-coupling between surface plasmons on opposite sides, with consequent generation of lower-surface plasmons. The narrow range of wavelengths is determined by the corrugation periodicity and can be chosen by design to contain the fluorescence emission wavelength of interest. Thus, optical energy at the fluorescence emission wavelength is transmitted through the film, which otherwise remains opaque to photons and thus to most background light.

Below the buffer layer is a sensing layer, which can be a semiconductor p/n junction or other electronic device that exhibits a measurable change in voltage, current, or resistance when it absorbs energy from plasmons. The buffer dielectric layer is thin enough to allow penetration of the surface plasmon electric fields into the sensing layer. Optionally, one can dispense with the buffer dielectric layer, in which case the sensing layer also serves partly as the lower dielectric layer.

This work was done by Margaret L. Tuma of Lewis Research Center and Russell W. Gruhlke of Ohio Aerospace Institute. Further information is contained in a TSP [see page 1].

Inquiries concerning rights for the commercial use of this invention should be addressed to NASA Lewis Research Center, Commercial Technology Office, Attn: Tech Brief Patent Status, Mail Stop 7–3, 21000 Brookpark Road, Cleveland, Ohio 44135. Refer to LEW-16368.

Calculating Chemical-Reaction Rates From Thermodynamic Data

Gas-phase chemical-kinetic rates are well approximated by a simple equation.

Lewis Research Center, Cleveland, Ohio

Kinetic rate data are needed to design all chemical processes. Specifically, they are needed to determine such things as ignition delay times, combustion times, and explosion limits in engine combustors. Previously, chemical kinetic rate data have been determined experimentally by use of reactors at the desired operating conditions. However, such data are often difficult to obtain.

A scheme for relating chemical kinetic rates to thermodynamic-property data has been developed. The scheme is based on the discovery that the rate, r, of a chemical reaction is related to the Gibbs gradient with respect to the extent of conversion, X, by

$$r = D\left[\exp\left(\frac{-1}{RT}\frac{\partial G}{\partial X}\right) - 1\right]$$

where the single constant D is used for all reactions, R is the universal gas constant, T is the absolute temperature, and G is the Gibbs energy. Using this equation, the chemical rate constants for each reaction can be related to the equilibrium constant for that reaction, and the net chemical rate can be predicted.

Ordinarily, energy levels from the thermodynamic data are used to calculate equilibrium compositions and not dynamic rates. The equilibrium condition for a given reaction is a balance between the forward and reverse rates for that reaction. When the system of reacting species is not in equilibrium, G is at a value higher than its minimum, and the rate is related to the difference between the actual and minimum values.

Data on the heat capacities, standard-state enthalpies, and Gibbs energies under equilibrium conditions were previously calculated for 1,130 chemical species and tabulated. These data can now be used for each chemical-reaction step to determine its rate. Using the present method, kinetic rates that have not yet been determined can be computed, enabling prediction of alternative chemical processes.

For comparison of experimental data with predictions by the present thermodynamic method, the Lewis General Chemical Kinetics and Sensitivity Analysis (LSENS) computer code was modified to incorporate the present method. The method was tested on the H/Br system with excellent results. In a similar test on the H/O system, the deviation between the predictions and the experimental data was greater for the present method than for the classical method. However, the disadvantage of the greater deviation in the present method may be offset by the advantage that one can use only the single constant D for all reactions, whereas in the classical method, one must use at least two constants (the preexponential factor and the activation energy) for each reaction to describe a given chemical system.

It will be necessary to demonstrate the present method on other chemical systems. One difficulty lies in the inclusion of small quantities of intermediate species, the properties of which may not yet have been tabulated. However, thermodynamic properties can be accurately estimated, given molecular structures. More work is being done to test the limits of the present thermodynamic method for kinetics. When completely verified, this method will have a widespread effect on the chemical industry.

This work was done by C. John Marek of **Lewis Research Center**. *Further information is contained in a TSP [see page 1].*

Inquiries concerning rights for the commercial use of this invention should be addressed to NASA Lewis Research Center, Commercial Technology Office, Attn: Tech Brief Patent Status, Mail Stop 7–3, 21000 Brookpark Road, Cleveland, Ohio 44135. Refer to LEW-16501.

Proximity Measurement of Pressure and Temperature

Electrical contact would not be necessary for interrogating submillimeter resonant microbeams.

NASA's Jet Propulsion Laboratory, Pasadena, California

Inexpensive, high-performance, optically coupled temperature and strain gauges based on a combination of advanced optoelectronic and microelectromechanical concepts have been proposed. The sensors would contain vibrating beams with submillimeter dimensions, made primarily of silicon by microfabrication techniques. The beams would be designed so that (1) their resonance frequencies would vary with strain and temperature, respectively, and (2) their vibrations would be both excited and measured by use of light. The sensors would be impervious to mechanical shocks, would have masses in the microgram range, and would consume only femtowatts of power. Unlike electrically coupled sensors, the proposed sensors would be immune to (and would not generate) electromagnetic interference at suboptical frequencies.

These sensors were conceived for original application in measuring strains and temperatures on a canister that would be sealed pyrotechnically on Mars to bring a sample of the Martian atmosphere back to Earth. The strain measurements would be converted to readings of the pressure of the enclosed gas sample. In that application, there is a requirement for noninvasiveness; one must not create a potential leak by penetrating the canister to insert instrumentation for monitoring the enclosed gas. There is also a requirement to be able to separate the canister from, and connect the canister to, different instrumentation systems without having to make and break sensor electrical contacts. The same features that make the proposed sensors attractive for the original application also make these sensors attractive for terrestrial applications for monitoring temperatures and strains in sealed gas containers and in other structures.

A sensor of this type would include either a cantilever or a double-pinned microbeam in a polycrystalline silicon vacuum enclosure. The sensor would include an integral photodiode, and in the presence of optical excitation, the electrical output of the photodiode would cause bending of the beam via electrostatic attraction. The vibrations would give rise to modulation of the incident light reflected from the beam. Optical excitation and readout would be accomplished via an optical fiber, which could be terminated in the sensor body or, if necessary, at a distance of as much as a few millimeters.

A double-pinned microbeam would be particularly suitable for measuring axial strain; if a sensor containing such a microbeam were intimately coupled to, and suitably oriented on, a structural member, the stress in the member would alter the tension in the beam, thereby altering its resonance frequency. A cantilever microbeam would be well suited for measuring temperature; the coefficient of thermal expansion of a bimorph coating can be made to differ from that of silicon, so that thermally induced stress in the beam would change its resonance frequency. Moreover, with a typical resonance quality factor (Q) of about 10^5 and power dissipation of about 10^{-15} W, a cantilever-microbeam temperature sensor would not thermally contaminate its environment.

This work was done by Frank Hartley of Caltech for **NASA's Jet Propulsion Laboratory**. *Further information is contained in a TSP [see page 1].*

NPO-20223

Adjacent-Pair Imaging Shearography Using Bacteriorhodopsin

In a developmental technique of real-time adjacent-pair imaging shearography, a thin film of bacteriorhodopsin is used to record shearograms in argon-laser light for immediate readout in helium/neon-laser light. Unlike conventional silver-halide-based photographic film, bacteriorhodopsin can be used as a real-time recording medium because it yields an image immediately upon exposure and is optically erasable. Bacteriorhodopsin also offers the advantage of resolution as high as 5,000 lines/mm — comparable to the resolutions of silver-halide-based films and much greater than the 80 lines/mm typical of the charge-coupled-device video cameras used heretofore in real-time shearography. Issues to be addressed in subsequent development include the difficulty of recording over a previously recorded image at the recording wavelength, the need for Fourier-transform optics for readout, the need to optimize the optics to realize the full potential for high resolution, and the relative insensitivity of bacteriorhodopsin film (about a tenth of that of silver-halide-based film).

This work was done by Colleen Fitzpatrick of Rice Systems, Inc., for **Kennedy Space Center.** *Further information is contained in a TSP [see page 1].*

In accordance with Public Law 96-517, the contractor has elected to retain title to this invention. Inquiries concerning rights for its commercial use should be addressed to

Colleen Fitzpatrick
Rice Systems,Inc.
1150 Main Street, Suite C
Irvine, CA 92614
(714) 553-8768
E-mail: ricesys@prodigy.com

Refer to KSC-11838, volume and number of this NASA Tech Briefs *issue, and the page number.*

Books and Reports

Potential Commercial Applications From Microgravity Combustion Research

The paper entitled "Potential Commercial Applications From Combustion and Fire Research in Space" reviews the status of potential commercial applications derived from research on combustion in microgravity environments encountered in orbiting spacecraft. Such research contributes to the understanding of basic combustion processes, including those that occur in normal Earth gravity. In microgravity, buoyancy-induced flow is nearly eliminated. Forces and resultant flows that are weak and are obscured under normal Earth gravity can be isolated, and temporal and spatial scales can be expanded. Because of the great economic importance of combustion processes, there is strong motivation to seek commercial applications of findings from microgravity-combustion research. Toward this end, the paper summarizes results from microgravity-combustion experiments, then briefly surveys applications and opportunities. Research topics discussed include solid-surface combustion, droplet combustion, and formation of soot. Potential applications include fire safety in spacecraft and terrestrial systems, innovative combustor designs for aerospace and ground propulsion systems, sensors and controls for combustion processes, and formation of advanced materials by use of combustion-synthesis processes.

This work was done by Robert Friedman and Valerie J. Lyons of **Lewis Research Center.** *To obtain a copy of the paper, "Potential Commercial Applications From Combustion and Fire Research in Space," see TSP's [page 1].*

Inquiries concerning rights for the commercial use of this invention should be addressed to NASA Lewis Research Center, Commercial Technology Office, Attn: Tech Brief Patent Status, Mail Stop 7-3, 21000 Brookpark Road, Cleveland, Ohio 44135. Refer to LEW-16538.

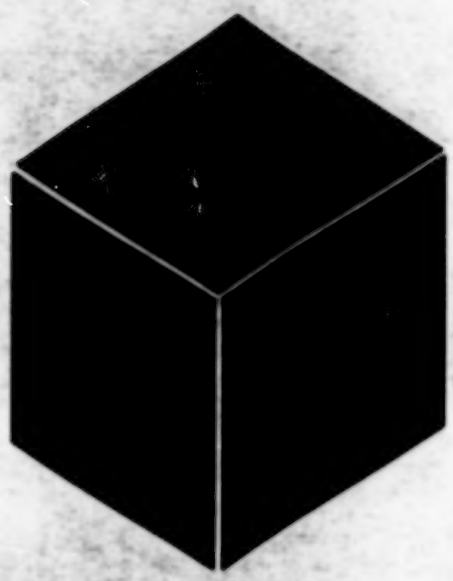

Materials

Hardware, Techniques, and Processes

25 Self-Lubricating Composite Coating for High-Temperature Use

25 Sputter Deposition of Pure and Fluoropolymer-Filled Al_2O_3

Books and Reports

26 Characterization of Woven-Carbon/Copper-Matrix Composites

BLANK PAGE

Self-Lubricating Composite Coating for High-Temperature Use

This material offers advantages over a previously developed similar material.

Lewis Research Center, Cleveland, Ohio

PS300 is a self-lubricating solid coating material for use in sliding contacts at temperatures up to 800 °C. PS300 is a composite of metal-bonded chromium oxide with barium fluoride/calcium fluoride eutectic and silver as solid lubricant additives. The "PS" in the name of this and other self-lubricating, high-temperature composite materials that have been reported in *NASA Tech Briefs* signifies that the material is applied to a substrate by plasma spraying of a powder blend of its constituents.

PS300 is similar to a previously developed material of this type, called "PS200." The main difference between the two materials is that instead of metal-bonded chromium oxide, the major constituent of PS200 is metal-bonded chromium carbide (see table). In either material, the major constituent serves as a tough, wear-resistant matrix. The additives provide lubrication by virtue of their low shear strengths. In particular, silver lubricates at low temperatures; at higher temperatures, where silver is too soft to support an appreciable load, the fluoride eutectic phase softens and behaves plastically.

The big disadvantage of PS200 is high cost. The metal-bonded chromium carbide is a highly processed, expensive constituent, and the presence of chromium carbide makes it necessary to resort to costly diamond grinding to polish the coating to the requisite finish prior to use. Moreover, at temperatures above 800 °C in air, the chromium carbide oxidizes, with a resultant increase in friction and loss of resistance to wear.

Composite Coating Material	Constituents and Proportions							
	Metal-Bonded Cr_2O_3*		Metal-Bonded Cr_3C_2**		Ag		BaF_2/CaF_2 Eutectic	
	Weight Percent	Volume Percent	Weight Percent	Volume Percent	Weight Percent	Volume Percent	Weight Percent	Volume Percent
PS300	80	80.3			10	5.5	10	14.2
PS200			80	77.1	10	6.4	10	16.5

* By Weight Percent, $80Cr_2O_3$+16Ni+4Cr
** By Weight Percent, $84Cr_3C_2$+3Ni+12Co+2Mo+2Al+1B+1Si

The Compositions of PS300 and PS200 are similar, the major difference lying in the metal-bonded, chromium-based constituent. PS300 offers advantages of lower cost and less difficulty in processing.

The metal-bonded chromium oxide in PS300 costs less than does the metal-bonded chromium carbide in PS200. Metal-bonded chromium oxide can be ground and polished by silicon carbide tools, eliminating the need for diamond finishing. Inasmuch as the chromium in PS300 is already in an oxidized state, the coating has potential for better tribological performance in air at high temperatures. Yet another advantage of PS300 over PS200 is that at high temperatures, chromium oxide is a good solid lubricant. Finally, in comparison with PS200, PS300 exhibits less of a tendency to clog spray-gun ports and can thus be plasma-sprayed more easily.

PS300 and PS200 have been tested under identical conditions on a pin-on-disk tribometer. In tests at temperatures up to 650 °C in air, the two materials exhibited comparable friction and wear properties.

This work was done by C. DellaCorte and B. J. Edmonds of **Lewis Research Center.** *Further information is contained in a TSP [see page 1].*

Inquiries concerning rights for the commercial use of this invention should be addressed to NASA Lewis Research Center, Commercial Technology Office, Attn: Tech Brief Patent Status, Mail Stop 7–3, 21000 Brookpark Road, Cleveland, Ohio 44135. Refer to LEW-16413.

Sputter Deposition of Pure and Fluoropolymer-Filled Al_2O_3

Transparent coats of Al_2O_3 could protect plastic windows.

Lewis Research Center, Cleveland, Ohio

Experiments have shown that nonreactive ion-beam sputtering can be used to deposit a transparent film of aluminum oxide on a polycarbonate, silicon, or fused-silica substrate. Similar experiments have shown that reactive ion-beam sputtering can be used to form a transparent film of either aluminum oxide alone or else aluminum oxide filled with a few percent of polytetrafluoroethylene (PTFE). The properties of reactively deposited Al_2O_3 films appear to be superior to those of nonreactively deposited Al_2O_3 films with respect to the intended applications, as explained below.

These experiments were conducted as parts of continuing efforts to develop hard, adherent, hydrophobic oxide films to protect polymeric windows (e.g., in automobiles and aircraft) against oxidation and abrasion and to enhance their ability to shed water. Earlier efforts along this line of development were reported in "Deposition of Sapphire by Conversion Coating" (LEW-15758), *NASA Tech Briefs*, Vol. 20, No. 8 (August 1996), page 68.

The deposition apparatus (see figure) was housed in a vacuum chamber and contained two ion sources: one that generated a beam of argon ions at a kinetic energy of 1,000 eV and one that generated an oxygen/argon plasma with an ion kinetic energy of about 170 eV. For nonreactive sputter deposition, the argon-ion beam was aimed at an aluminum oxide sputtering target and the oxygen/argon ion source was not used. For reactive sputter deposition, the argon-ion beam was aimed at an aluminum sputtering target, while the oxygen/argon-ion beam was aimed at the deposition substrate. The addition of PTFE during reactive

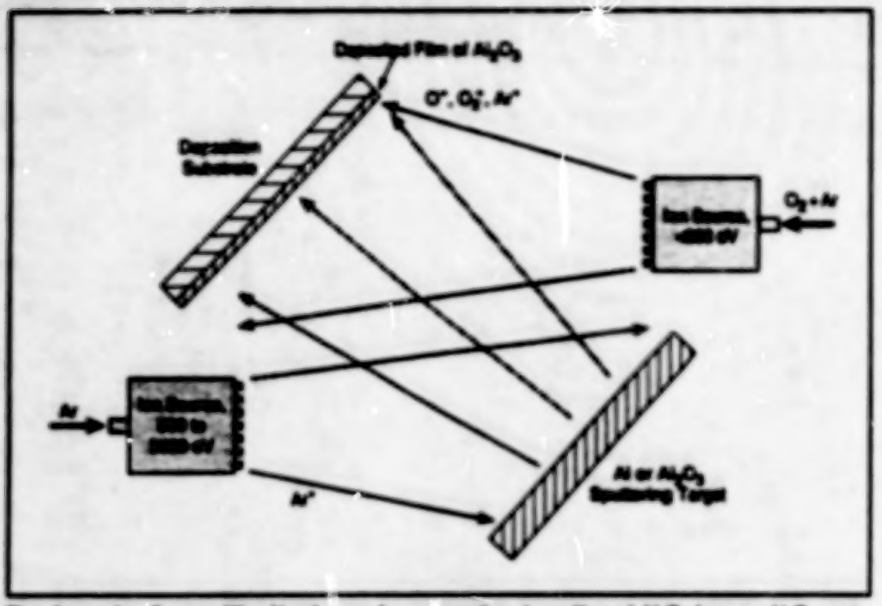

The Argon-Ion Source Was Used Alone for Nonreactive Deposition of Al_2O_3 from an Al_2O_3 Sputtering Target or With the Oxygen/Argon Source for Reactive Deposition of Al_2O_3 from an Al Target.

sputtering was accomplished by placing a wedge of PTFE onto the aluminum sputtering target. In one experiment, a film of PTFE (only) was deposited by use of a PTFE (only) sputtering target.

In each case in which a film was deposited on a fused-silica substrate, part of the substrate was masked with tape to provide a datum surface for measurement of the thickness of the deposit by use of a profilometer. Typical thicknesses of Al_2O_3 films ranged from 1,600 to 2,700 Å. A deposit of 92 percent Al_2O_3 and 8 percent PTFE was found to be 3,800 ± 260 Å thick, and a deposit of PTFE alone was found to be 12,300 ± 1,077 Å thick. Water contact angles were also measured on the fused-silica substrates. In cases in which films were deposited on silicon substrates, the intrinsic stresses in the films were determined by measuring the changes in the surface bows of the substrates. Spectral transmissivities of uncoated and coated fused-silica and polycarbonate substrates were measured. Qualitative tests of resistance to abrasion were performed on two types of polycarbonate substrates: uncoated and one reactively coated with Al_2O_3 to a thickness of 12,200 Å.

Stresses were found to be slightly lower in reactively deposited than in nonreactively deposited Al_2O_3 films. Stresses were reduced by incorporation of PTFE. Unexpectedly, films of Al_2O_3 + PTFE were found to be less hydrophobic than are films of Al_2O_3 alone — an effect that might be attributable to the formation of aluminum fluoride. In comparison with nonreactively deposited Al_2O_3, reactively deposited Al_2O_3 proved to be slightly more hydrophobic and more optically transmissive in the ultraviolet. The addition of PTFE exerted little effect on transmittance. The 12,200-Å-thick Al_2O_3 reactively deposited Al_2O_3 films on polycarbonate were found to increase the absolute absorptance by only about 1.8 percent while providing some resistance to abrasion by small particles like those typically encountered during cleaning of windows and lenses. Thus, it appears that reactive ion-beam sputtering of Al_2O_3 is potentially useful as a technique to apply clear, abrasion-resistant films to polymeric windows and possibly other optical components.

This work was done by Sheron K. Rutledge and Bruce A. Banks of Lewis Research Center and Jason Hunt of Ohio Aerospace Institute. Further information is contained in a TSP [see page 1].

Inquiries concerning rights for the commercial use of this invention should be addressed to NASA Lewis Research Center, Commercial Technology Office, Attn: Tech Brief Patent Status, Mail Stop 7–3, 21000 Brookpark Road, Cleveland, Ohio 44135. Refer to LEW-16424.

Books and Reports

Characterization of Woven-Carbon/Copper-Matrix Composites

Designing metal-matrix composites into actual components requires both experimental and analytical characterization of the behavior of these composites. This report describes mathematical modeling and experimental characterization of the elastoplastic behaviors of composite materials made of copper and copper-alloy matrices reinforced with carbon fibers in a biaxial weave known in the industry as "8-harness satin." The experiments included monotonic- and cyclic-tension and -compression tests, combined tension/compression tests, and monotonic- and cyclic-shear tests, with strain gauges attached to specimens oriented variously with the fill or warp directions of the weaves along the directions of applied stresses. The tests yielded data on initial moduli, yield stresses, post-yield behaviors, effects of sizes and placements of strain gauges, effects of alloying to improve fiber/matrix bonding, yield surfaces, and failure mechanisms. The mathematical-modeling effort included an extension of a previously developed repeating-three-dimensional-unit-cell model of the micromechanics of a composite material to incorporate effects of inhomogeneity and plasticity at the subcell level. The model is used to examine the effects of porosity, refining the representative geometry, altering the fiber volume fraction, and changing the size and placement of a strain gauge, all upon the mechanical responses of a composite. The predictions of the model are compared with the results from the monotonic-stress tests.

This work was done by Brett A. Bednarcyk, Christopher C. Pauly, and Marek-Jerzy Pindera of the University of Virginia for Lewis Research Center. To obtain a copy of the report, "Experimental Characterization and Micromechanical Modeling of Woven Carbon/Copper Composites," see TSP's [page 1].

Inquiries concerning rights for the commercial use of this invention should be addressed to NASA Lewis Research Center, Commercial Technology Office, Attn: Tech Brief Patent Status, Mail Stop 7–3, 21000 Brookpark Road, Cleveland, Ohio 44135. Refer to LEW-16540.

Computer Programs

Materials

27 ICAN/PART — Integrated Particulate Composite Analyzer

Mathematics and Information Sciences

27 Web-Based Software for Coordinating Work

27 Virtual-Reality Platform-Independent Software for Access to Mars Data

BLANK PAGE

Computer Programs

These programs may be obtained from COSMIC. Please contact

COSMIC
Computer Services Annex
University of Georgia
Athens, GA 30602
Telephone No. (404) 542-3265.

Materials

ICAN/PART — Integrated Particulate Composite Analyzer

This program computes properties and stresses at the constituent and composite levels.

The Integrated Particulate Composite Analyzer (ICAN/PART) computer program is a modified version of the Integrated Composite Analyzer (ICAN) program (LEW-15592/LEW-15832), which was developed to conduct analyses of the micromechanics of fiber-reinforced polymer-matrix composite materials. ICAN/PART is a computationally efficient computer code that can be used by engineers in both aerospace and nonaerospace fields to characterize and design particulate-reinforced composite materials. These composites are useful in circumstances in which multi-phased materials are desired but the costs and difficulties of manufacturing continuous-fiber-reinforced composites are too great.

ICAN/PART can compute the effective properties and constituent microstresses of a particulate-reinforced composite as well as of a fiber-reinforced composite that includes a particulate-reinforced matrix material. The user obtains preliminary information on the order of magnitude of stresses that will be found in a given load state. If more-detailed information about the specific stress levels in specific locations of a composite-material object is required, a detailed finite-element model could then be constructed and analyzed.

The manner of using ICAN/PART is very similar to that of the original ICAN code. ICAN/PART includes a provision for a dedicated data bank that enables the user to build a database of properties of commonly used particle and binder materials. The user need only specify code names for constituents. Input includes code names or properties of constituent materials, and factors that reflect the process of fabrication and the geometry of the composite-material object. Output includes the various ply and composite properties, composite structural response, and composite-stress-analysis results with details of failure.

ICAN/PART is written in FORTRAN 77. Two machine versions are available. The Unix-based version, LEW-16460, has been successfully implemented on a Sun4 SLC computer running SunOS 4.1.3_U1, a Sun4 IPC running Solaris 2.4 (SunOS 5.4), and an SGI Indigo2 computer running IRIX 6.2. The IBM PC-based version, LEW-16484, has been successfully run on a '486 microprocessor running MS-DOS 5.0, a '486 microprocessor running Windows95, and a Pentium microprocessor running Windows95. The code has been successfully compiled under Microsoft's Fortran Powerstation 1.0. A sample executable code is provided. The standard distribution medium for the Unix-based version is a 3.5-in. (8.89-cm), high-density diskette in Unix TAR format. The standard distribution medium for the IBM PC version is a 3.5-in. (8.89-cm), high-density diskette in PC format. Alternate distribution media are available on request. ICAN/PART was released to COSMIC in 1997.

This program was written by P. L. N. Murthy and R. K. Goldberg of **Lewis Research Center** *and S. K. Mital of the University of Toledo.*

For further information on the Unix version, see TSP's [page 1].
LEW-16460

For further information on the IBM PC-based version, see TSP's [page 1].
LEW-16484

Mathematics and Information Sciences

Web-Based Software for Coordinating Work

WWWorkflow is a language-driven, database-mediated, web-based process mediation system. WWWorkflow leverages on intranet applications and existing information infrastructure services, making it possible to add workflow management features to preexisting information management systems, without the need for significant modifications of those systems. A distinctive feature of WWWorkflow is the careful separation of process mediation from product-data management. WWWorkflow supports many types of workflow and is not focused on any single information structure. WWWorkflow components include a web-based user front-end, a workflow "engine," a workflow data base, and a graphical workflow editor and authoring tool. The web-based user front-end of WWWorkflow allows any user with a web browser to interact with the system. The workflow "engine" contains a workflow language interpreter, as well as an event-driven process mediation service. The workflow data base provides persistence of workflows underway as well as status and historical information for complete reporting. The graphical workflow editor and authoring tool provides both capabilities to produce and edit workflow procedures.

This program was written by Charles Ames, Scott Burleigh, and Stephen Mitchell of Caltech for **NASA's Jet Propulsion Laboratory**. *Further information is contained in a TSP [see page 1].*

This software is available for commercial licensing. Please contact Don Hart of the California Institute of Technology at (818) 393-3425. Refer to NPO-20124.

Virtual-Reality Platform-Independent Software for Access to Mars Data

The Virtual Reality Mars Atlas User Interface (VR-MAUI) provides an atlas-like interface for access to Mars data. This access is provided via the World Wide Web, using JAVA. Within VR-MAUI, images are organized as maps. These maps provide a natural coordinate system, which defines feature locations. VR-MAUI is used to (1) examine, process, display, and analyze variable-resolution images of Mars and (2) interactively create VRML models of the Martian surface. VR-MAUI provides a point-and-click interface for selecting a specific location on Mars. Users identify locations by image features, pixel coordinates, or map coordinates. Data can be displayed in the forms of text, maps, still images, movies, and VRML models.

The current version of VR-MAUI provides an interface to *Viking* and Mars *Pathfinder* data. Future versions will provide similar access to other objects in

the solar system. When fully developed, VR-MAUI will (1) display planetary surfaces and atmospheres in three dimensions using VRIM and (2) display and analyze spacecraft and instrument data during flight operations.

This program was written by Raymond J. Bambery, Eric M. DeJong, Steven R. Levoe, and Myche McAuley of Caltech for NASA's Jet Propulsion Laboratory. Further information is contained in a TSP *[see page 1].*

This software is available for commercial licensing. Please contact Don Hart of the California Institute of Technology at (818) 393-3425. Refer to NPO-20173.

Mechanics

Hardware, Techniques, and Processes

33 Fixtured Spheres for Training in Simulated Weightlessness
34 Applying Controlled Pressure Distributions to Complex Curved Surfaces
34 Increased Life for Steel-Slitter Guide Rolls

Books and Reports

35 Equations for Failure Modes of Mechanical Systems

BLANK PAGE

Fixtured Spheres for Training in Simulated Weightlessness

This inertial properties of these neutrally buoyant spheres would approximate those of objects to be simulated.

Lyndon B. Johnson Space Center, Houston, Texas

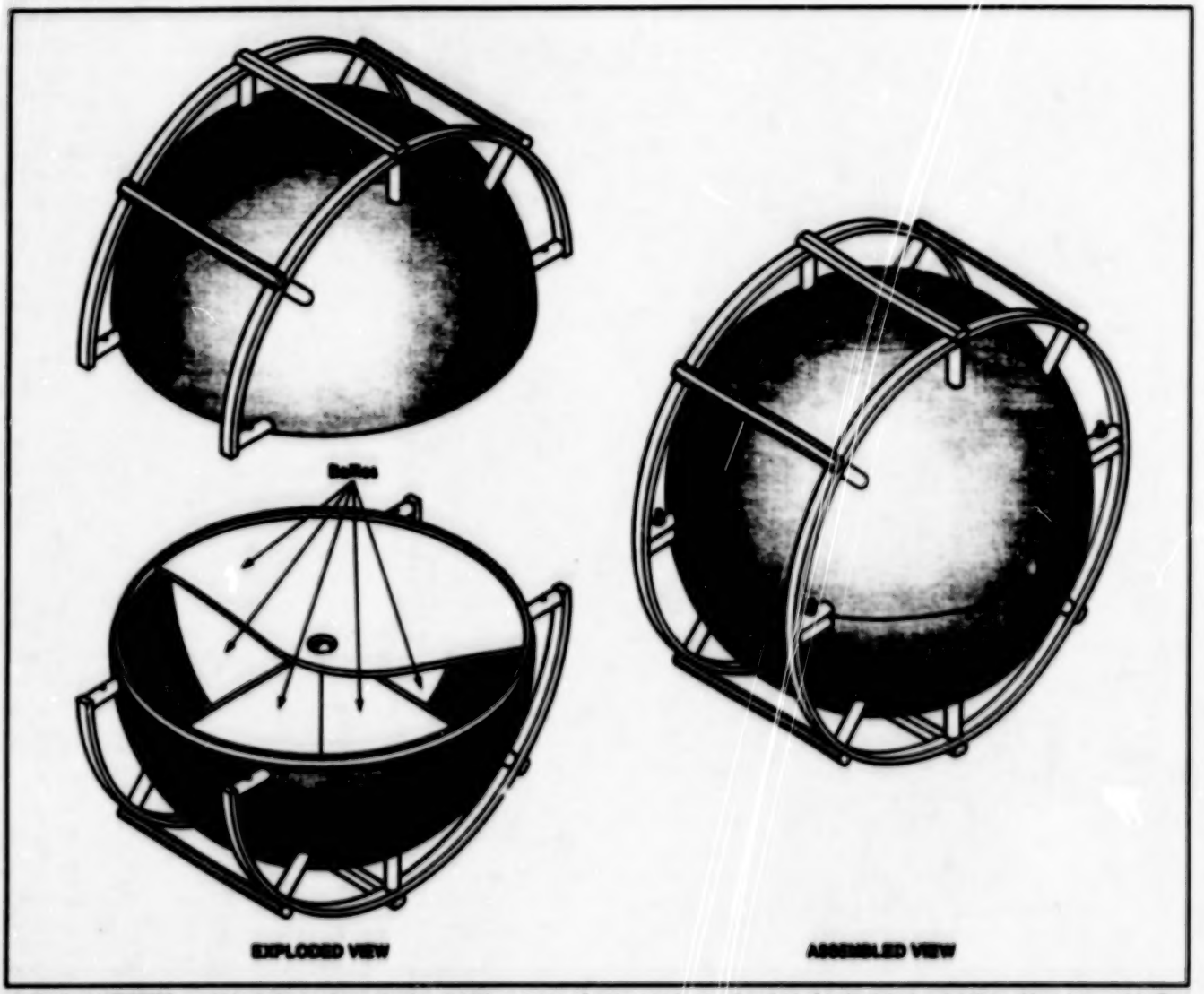

A Typical WETFITS would include a sphere sized to contain a mass of water nearly equal to that of a simulated weightless object. Internal baffles would help to approximate the rotational inertia of the object.

Weightless Environment Training Facility Inertial Training Spheres (WETFITSs) are proposed neutrally buoyant training tools that would be used in NASA's Weightless Environment Training Facility (WETF), where astronauts are trained underwater to manipulate objects in zero gravitation. Heretofore, the training in the WETF has provided astronauts accurate simulations of visual conditions but has not addressed the feel of manipulating objects. The WETFITSs are intended to address the issue of feel; more specifically, each WETFITS would be designed so that its inertial properties underwater would approximate those of a simulated object with a specified mass and six degrees of freedom in zero gravitation. A WETFITS (see figure) could be sized to simulate any large mass to be manipulated in zero gravitation, could be designed and manufactured cost-effectively, and would be reusable.

In WETF practice that continues to this day, the neutral buoyancy needed to simulate zero gravitation underwater is achieved by attaching polystyrene foam and lead weights to astronauts, equipment, and mock-ups of simulated objects. In so doing, no attempt is made to approximate the masses and other inertial properties of simulated weightless objects and, as a result, astronauts usually do not get an accurate feel for handling the objects in zero gravitation.

The WETFITS concept eliminates the need for lead weights and polystyrene foam. Instead, one would use a volume of water to approximate an object with a specified mass and make it close to neutrally buoyant. A sphere was chosen for the shape of the volume to minimize the drag force created by moving the object through the water in any direction. The sum of (a) the mass of the water in the sphere and (b) the extra apparent mass from boundary-layer generation would approximate the mass of the simulated object. A WETFITS would include internal baffles to enable some simulation of rotational inertia.

This work was done by Kathryn M. Miller, Michael J. Stagnaro, Christophis Lovchik, Dominic DeRosso, and Pierre Thuot of **Johnson Space Center**. *No further documentation is available.*
MSC-22501

Applying Controlled Pressure Distributions to Complex Curved Surfaces

A straightforward technique involves airbags restrained by nets.

Lyndon B. Johnson Space Center, Houston, Texas

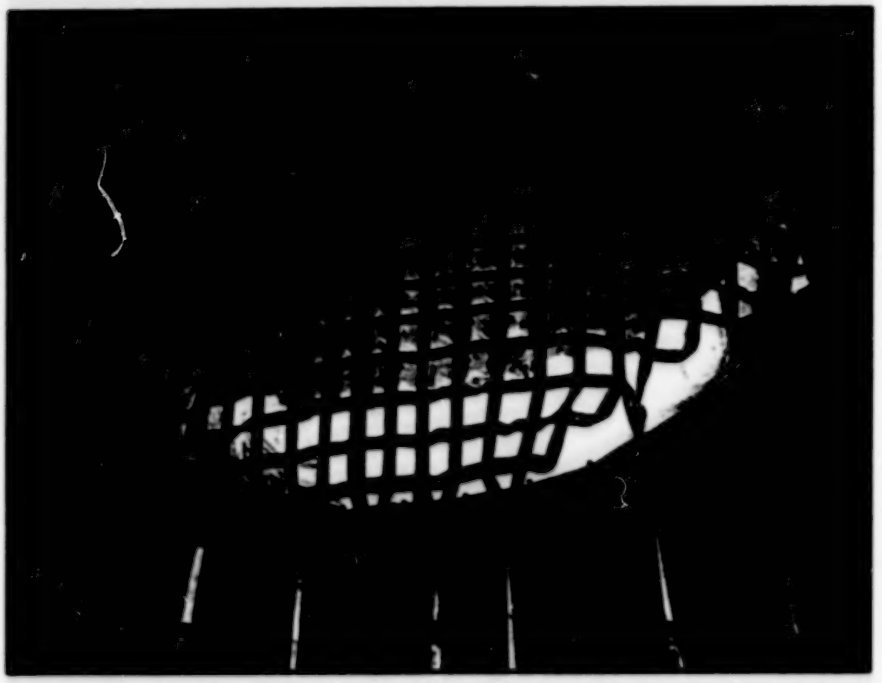

An Assembly of Airbags Restrained By a Net applies pressure to an aerodynamic test surface — in this case, simulating aeropass loads on the surface of a spacecraft aerobrake.

A technique for applying controlled test pressures to curved surfaces is based on a principle similar to that of a compartmented pilot's or astronaut's pressure suit. The technique involves the use of airbags that accommodate geometric complexity in both the surface under test and in the spatial variation of the pressure to be applied. This method also provides the enhanced capability to vary the pressure locally, refining the load distribution at the airbag interfaces.

Previous methods for applying pressure loads have involved the use of point-load actuators distributed over the test surface. In using this technique, especially with surfaces of complex curvature, the controllability of the actuators with respect to directions of the loads that they apply is limited and the concentrated load at the actuator locations is a poor approximation of the desired pressure distribution. In a technique similar to the present method, pressure is applied to the test surface via an airbag restrained by a negative mold of the surface. However, this technique requires the expense of constructing the mold and the mold leaves little flexibility to adapt to the variations in shape of the test surface.

In the present method, one or more airbags are restrained against the test surface by use of a custom-fitted net (see figure). The quantity, size, and inflation pressure of each of the airbags can be adjusted to obtain a sufficiently accurate approximation of the required pressure distribution. Airbag geometry is sized by the maximum deflection of the net and the deflections of the structure. The net system includes a means of adjustment to compensate for net stretching and control of net separation from the structure. Ratchet mechanisms secure the net to the ground or to a suitable framework and serve as means of adjusting preloads to control deflections of the airbags.

This work was done by Michael C. Eubanks, John J. Zipay, and Edgar O. Castro of **Johnson Space Center**. *Further information is contained in a TSP [see page 1].*
MSC-22352

Increased Life for Steel-Slitter Guide Rolls

Wear-resistant sleeves are press-fit onto shafts.

Lewis Research Center, Cleveland, Ohio

There has been some success in continuing efforts to increase the service lifetimes of the guide rolls in hot-roll-slitter machines in the steel industry. In these machines, hardened knives are used to slice sheets of steel from large steel coils. The sheets are up to 0.375 in. (9.525 mm) thick and have various lengths and widths. A steel coil to be cut is positioned in a hot-roll-slitter machine by use of four guide rolls (two on each side) that spin as the steel passes between them on the way to the knives. The guide rolls are thus subjected to harsh grating and scraping conditions as well as high-pressure rubbing and friction as the coil is unwound to be sliced. Consequently, deep grooves are quickly worn into the guide rolls, making it necessary to replace the guide rolls and thereby causing several hours of down time.

Guide rolls of modified design were constructed in an initial effort to increase the longevity and usefulness of the guide rolls and to reduce slitter-machine down time for changing of guide rolls. Each such guide roll included a shaft fabricated from 4140 steel, plus a sleeve that was machined, then pressed onto the shaft. A collar was added to key the sleeve in place. Then, to make the sleeve more resistant to wear, an abrasive-resistant material (PS-212) about 0.015 in. (0.38 mm) thick was plasma-sprayed onto the sleeve. In tests, the average life span of these rolls was found to be more than double that of rolls of the original, unmodified design. However, a new failure mode occurred; the coatings eventually became detached from the sleeves.

In a second modified design (see figure), each roll was equipped with a shell sleeve made from a more wear-resistant tool steel (D-2), which was machined and then heat-treated for longer wear life. In tests on slitter machines, the life spans of rolls of this second modified design were found to be increased by factors of at least four to five. In addition, the time needed to change the sleeves was reduced greatly.

and the reduction in cost of changing sleeves (in comparison with changing entire rolls) was found to be substantial. Therefore, until a more-compatible coating can be found and proven advantageous in tests, rolls of the heat-treated shell-sleeve design are in use on the affected slitter machines, saving time and money.

This work was done by Richard Soltis and William Waters of Omni Corp. and Darryl Bruck of Diversity Manufacturing Co. for **Lewis Research Center**. *No further documentation is available.*

Inquiries concerning rights for the commercial use of this invention should be addressed to NASA Lewis Research Center, Commercial Technology Office, Attn: Tech Brief Patent Status, Mail Stop 7–3, 21000 Brookpark Road, Cleveland, Ohio 44135. Refer to LEW-16534.

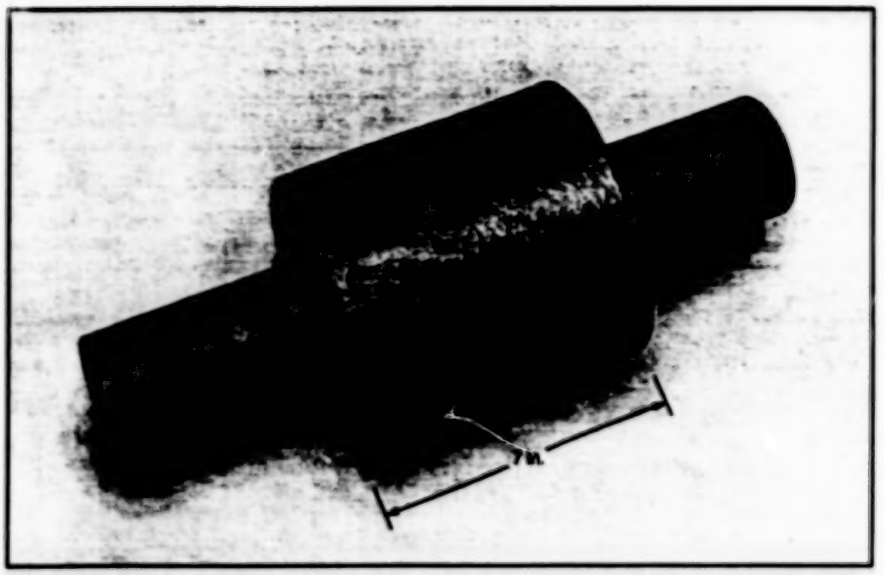

This Guide Roll for a slitting machine used in the steel industry features an improved shell-sleeve design.

Books and Reports

Equations for Failure Modes of Mechanical Systems

A report presents information compiled from a search of the literature on failure modes of mechanical systems. The report was written to provide a reference base for the application of first-order reliability methods to mechanical systems in the development of a system-level design methodology. In the report, each of 20 failure modes is assigned to one of four classes: wear, corrosion, fatigue, or material degradation. A brief description of each class and mode is presented. For each mode, there is a definition, plus a description of one or more failure mechanism(s) and/or one or more mathematical model(s). The mathematical models include equations, denoted "limit-state relationships," that describe such quantities as rates of wear or corrosion as functions of physical and chemical conditions and of relevant process variables. The limit-state relationships can be used in probabilistic reliability analyses of mechanical systems affected by the failure modes.

This work was done by Michael Kowal and Thomas Cruse of Vanderbilt University for **Lewis Research Center**. *To obtain a copy of the report, "Compendium of Mechanical Limit-States," see TSP's [page 1].*

Inquiries concerning rights for the commercial use of this invention should be addressed to NASA Lewis Research Center, Commercial Technology Office, Attn: Tech Brief Patent Status, Mail Stop 7–3, 21000 Brookpark Road, Cleveland, Ohio 44135. Refer to LEW-16497.

BLANK PAGE

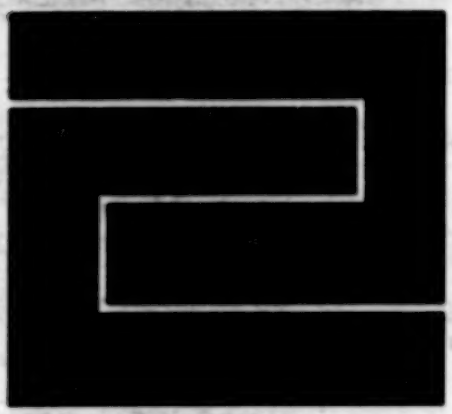

Fabrication Technology

Hardware, Techniques, and Processes

37 Friction Stir Weld System for Welding and Weld Repair
37 Rapid Prototyping of Cast Metal/Fiber Composites

BLANK PAGE

Friction Stir Weld System for Welding and Weld Repair

An improved apparatus takes the friction stir weld process to the manufacturing floor as a complete system.

Marshall Space Flight Center, Alabama

A friction stir weld (FSW) system for welding and weld repair can be used on the manufacturing floor, as well as in the laboratory environment. This FSW system can be used in a wide variety of welding and weld repair applications. It is capable of handling up to 6,000 pounds (26.7 kN) of axial load while operating within close tolerances.

This FSW system includes seven subcomponents: a base foundation unit (BFU), a hydraulically controlled elevation platform (EP), the hydraulically adjustable pin tool (HAPT), backplate tooling, fixturing, a roller mechanism, and the real-time adaptive computer numerical control (CNC) and process control system (APCS). Together, these subcomponents allow the FSW to be used on the manufacturing floor as a complete welding system.

The BFU is unique to accommodate the internal mechanical entities of the system. It is designed to operate under the radial and axial loads associated with the FSW process. The hydraulically controlled EP is the result of novel applications of existing technologies to create an elevation feature with three axes of movement, specially designed to function under operating pressures. This movement is necessary to attain the proper pin tool location with respect to the center of the weld joint. The HAPT is a standalone piece of hardware, which was integrated into the FSW system. (However, the positioning of the a & b axis around the N axis is unique.) The APCS component was specially designed to function as an integrated controller for a variety of functions and data gathering operations.

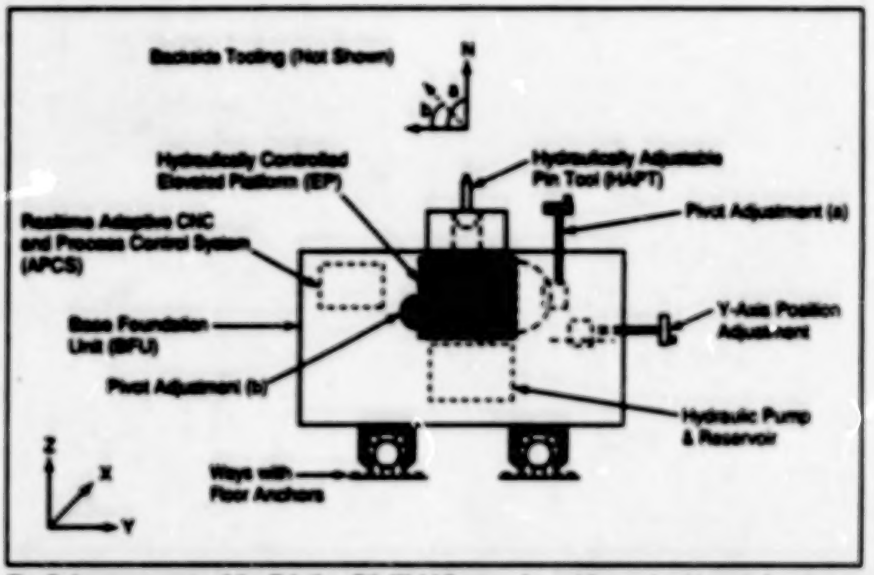

The Subcomponents of the Friction Stir Weld System for welding and weld repair function as one integrated welding system.

The novelty of the FSW System for welding and weld repair is the fact that the seven subcomponents act as one integrated welding system. This system has unlimited applications in manufacturing where welded structures are vital to the fabrication cycle. This apparatus provides the capability for initial welding and weld repair of friction stir welds and fusion welds.

This equipment is extremely energy efficient. A single-pass, 12.5-mm deep weld can be made in 6xxx series alloy using a gross power of no more than 3 kW. Also, the maintenance of this equipment is minimal, requiring no special operation or operator maintenance training. In addition, this machine tool is ideally suited to automation and integration with other machine-tool operations.

Another advantage of this system and its mode of operation is that there is no need for such consumables as filler wire or the shielding gas that is needed for welding aluminum alloys.

With this system, it is possible to make butt- and lap-seam welds between wrought, cast, and extruded materials, leading to simplification of manufacture.

Finally, the FSW process is a clean process, producing none of the health hazards such as welding fumes or radiation.

This work was done by Jeff Ding of Marshall Space Flight Center, Peter L. Romine of Florida International University, and Peter A. Colpoetz of Boeing North American, Inc. Further information is contained in a TSP [see page 1].
MFS-30125

Rapid Prototyping of Cast Metal/Fiber Composites

This process is a faster and more cost-effective method of prototype production.

Marshall Space Flight Center, Alabama

A rapid prototyping process enables the incorporation of continuous fiber reinforcement into a cast metal-matrix composite. In one older process, cast metal-matrix composites are made by introducing fibers or particles into molten or partially solidified metals, then casting the resulting slurries into molds. In an older process, masses of particles are preformed, then molten alloys are infiltrated into the masses. The alloys then freeze in the interstices, forming metal-matrix composites.

In the rapid prototyping process, fibers are inlaid into a wax model that is later shelled and cast. In a demonstration of the feasibility of the process, a fused-deposition apparatus was used to make a model tensile bar. For concept verification trials, the intervals between fibers were determined and grooves were carved into two tongue depressors at those predetermined intervals. Each tongue depressor was taped onto opposing ends of a sample wax model. A fiber was then placed into each groove of one tongue depressor and taped down. The fibers were then drawn across the build space and placed into the grooves of the tongue depressor on the other side and taped down. This

resulted in a frameline structure made of the fibers strung between the two ends.

This frameline structure was removed from the wax model and another one constructed using the same method. The fused-deposition apparatus was preprogrammed to pause between successive layer-building processes to enable the innovators to construct another frame.

For these trials, emphasis was placed on the applicability of producing continuous-fiber-reinforced metal-matrix composites by rapid prototyping. Therefore, a simple alignment of fibers previously proven to strengthen the part being built was used. However, there is a need to incorporate metal-matrix composites into regular production parts, and not into tensile-test bars only.

Although these concept verification trials involved linearly aligned fibers, the innovators are currently working on conceptual designs for circularly aligned fibers.

This work was done by Floyd E. Roberts and Erica Dudley of the **Marshall Space Flight Center**. *Further information is contained in a TSP [see page 1].*

Inquiries concerning rights for the commercial use of this invention should be addressed to the Patent Counsel, Marshall Space Flight Center [see page 1]. Refer to MFS-31180.

Mathematics and Information Sciences

Hardware, Techniques, and Processes

41 WAN DBMS Search Engine for Scientific Data Formats

42

BLANK PAGE

WAN DBMS Search Engine for Scientific Data Formats

New technology increases the efficiency of data analysis and retrieval.

NASA's Jet Propulsion Laboratory, Pasadena, California

A software interface between scientific data formats (SDF's) and wide-area database search-engine software has been developed to provide seamless access to data used in support of NASA projects. Most SDF's are known or understood by only a select audience. These SDF's are also only searchable using specialized tools unique to that particular SDF. This type of data storage and retrieval system excludes occasional users or management from easily accessing data products. Therefore, a simple access to data products has been developed based on the web browser paradigm.

Typically, a single host tracks data products using a commercial relational database management system (RDBMS) or custom file-based data base. With this type of (DBMS) data base management system, only references to products and fixed-file descriptors are allowed for data storage and retrieval. For this reason, a viewable data dictionary coupled with standard and familiar search tools were used to remove these limitations.

This innovative technology is a Search Engine System for Scientific Data Formats. It exists as several government off-the-shelf software (GOTS) and commercial off-the-shelf software (COTS) products, integrated to form a single, logical host for a distributed search tool.

This state-of-the-art search engine has been running on a developmental web site. Here, the webmaster designates an SDF directory, which is the repository for SDF files. The SDF directory is input to a translator program, which runs automatically with the webmaster's user name and privileges. The translator program extracts certain data, such as variables, attributes, file descriptions, time stamp, and a uniform resource locator (URL) for each SDF found in the tree below the specific directory. It then converts this data to a Hypertext Markup Language (HTML) document. The time stamp is used to update the HTML document if an SDF file changes. The system periodically submits new or changed URL's to commercial search engines. This system also allows nontext search extensions.

The capability to search the data dictionary of SDF's is a key innovation. Users who are unfamiliar with a library's structure are able to gain access to that structure, allowing them judge a data product's value.

The union of a WAN DBMS to SDF's is a second innovation. The WAN DBMS interfaces various search engines to the internally self-describing SDFs. This allows remote users to search SDF's using data element names, types, and values.

Simplified access to complex data bases lets users explore data intuitively. This enhances the value of the data by increasing their usefulness to the scientific community.

This work was done by John T. Robinson and Steven Pham of SARA, Inc., Electronics and Information Systems Business Area, for **NASA's Jet Propulsion Laboratory.** *For further information, contact John Robinson, SARA, Inc., 15262 Pipeline Lane, Huntington Beach, CA 92649-1136, Telephone: (714) 373-5509.*
NPO-30036

BLANK PAGE

Life Sciences

Hardware, Techniques, and Processes

47 Chemiluminescent Quantitation of Organic Compounds in Water

47 Image-Matching System Highlights Changes in Skin Lesions

BLANK PAGE

Chemiluminescent Quantitation of Organic Compounds in Water

Electrocatalyzed reactions generate light indicative of concentrations of selected compounds.

Lyndon B. Johnson Space Center, Houston, Texas

A method of measuring the concentration of a selected organic compound (analyte) in a sample of water involves (1) producing hydrogen peroxide as a byproduct of enzyme-catalyzed oxidation of the analyte, (2) producing light in an electrocatalyzed reaction of the hydrogen peroxide with luminol, and (3) measuring the intensity of this light. The method could prove useful in a variety of applications, including water-purification systems, closed environmental life-support systems, bioreactors, and other biotechnological systems.

The luminescent reaction is effected by feeding two aqueous streams into an electrocatalyzed-luminescence (ECL) cell (see figure). One stream carries luminol dissolved from a bed of luminol crystals. The rate of dissolution of luminol from the bed and the concentration of luminol in the water is maintained at the desired level by maintaining the pH of the water at 10.3; for this purpose, the flow of water is directed through basification modules containing MgO, both upstream and downstream of the luminol bed. (Rebasification downstream of the luminol bed is necessary because the dissolution of luminol neutralizes the solution.)

The other aqueous stream that flows into the ECL cell contains the analyte. If the analyte is H_2O_2, then this stream is fed directly to the ECL cell without further treatment. If the analyte is an organic compound or compounds, then this stream is first passed through a column containing an immobilized enzyme that catalyzes the oxidation of the analyte. For example, if the analyte is ethanol, then the enzyme is alcohol oxidase. The effluent from the column thus contains the products of the enzyme-catalyzed oxidation, including H_2O_2.

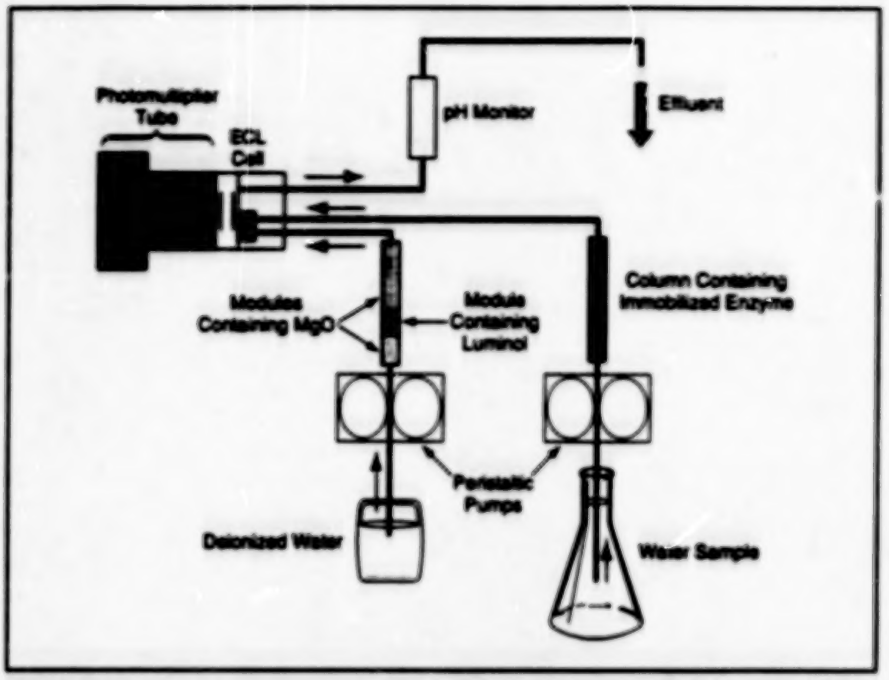

Light Is Produced in the electrocatalyzed reaction between (a) luminol and (b) H_2O_2, which is introduced into the sample stream by the enzyme-catalyzed oxidation of the analyte. The amount of light emitted is approximately proportional to the concentration of the analyte in the sample stream.

The two streams are mixed in the ECL cell. A controlled voltage across the cell catalyzes the oxidation of the luminol by hydrogen peroxide from the sample stream. A photomultiplier measures light emitted by this reaction. The intensity of this light is approximately proportional to the concentration of the analyte in the sample.

This work was done by Charles E. Verostko of Johnson Space Center *and James E. Atwater, James R. Akse, Jeffrey Dehart, and Richard R. Wheeler, Jr., of Umpqua Research Co. Further information is contained in a TSP [see page 1].*

This invention is owned by NASA, and a patent application has been filed. Inquiries concerning nonexclusive or exclusive license for its commercial development should be addressed to the Patent Counsel, Johnson Space Center [see page 1]. Refer to MSC-22605.

Image-Matching System Highlights Changes in Skin Lesions

Growth of moles is highlighted to prompt closer examination.

NASA's Jet Propulsion Laboratory, Pasadena, California

A video imaging and image-data-processing system for use in dermatological examinations acquires and processes images of patients' skins. The system processes a current image of a selected area of a patient's skin along with an image of the same area acquired previously, generating a comparison image that highlights any nevi (moles) that have appeared, disappeared, grown, and/or shrunk in the interim.

Most nevi are harmless, but changes into malignant melanoma can occur. Early detection is essential for effective treatment of malignant melanoma. Some patients have hundreds of nevi, so that it is difficult to track changes in the nevi that could signify the development of melanoma. The present image system assists the physician in identifying changes in nevi; the physician can then concentrate on examining any changed nevi.

The system includes a video camera, which is used to acquire the images. Typically, an image covers the patient's back from neck to waist. The first image of this area is digitized and stored on a computer disk. In a subsequent examination, a second image of the same area is digitized, stored, and processed along with the first image to generate the comparison image.

Because of differences between the ini-

ative alignments of the camera and patient in acquiring the two images, these images are not exactly registered with each other. Therefore, processing begins with the manual selection of a number (typically between 2 and 20) of nevi for use as landmarks in computing a nonlinear geometric transformation between corresponding points in the two images; the transformation is exact at the landmarks and a close approximation between them.

The average of the intensities of the central pixels of the landmarks in each image is computed, and is designated intensity A. The average of the intensities of all other pixels in each image is computed and designated intensity B. A linear transformation between the A and B intensities of both images is computed and used to correct the contrast between the images after they have been geometrically transformed into registration. A local shading correction is also applied: from the intensity of each pixel in each image, the median pixel intensity of all pixels in a small rectangular area around the pixel is subtracted.

From the shading-corrected, contrast-corrected intensity of each geometrically transformed pixel in the second image, the shading-corrected intensity of the corresponding pixel in the first image is subtracted. To bring negative values into the range of visibility, a middle gray-level intensity is then added to all pixels. The result is the comparison image. Wherever a nevus has grown or appeared between the time of acquisition of the first and second images, a dark spot is generated in the comparison image. Similarly, wherever a nevus has shrunk or disappeared, a bright spot can be seen in the comparison image.

Optionally, the comparison image can be rendered in false color to facilitate examination. Instead of adding a gray level, the negative changes in intensity (darkening changes, which could signify melanoma) are displayed in red, while positive changes in intensity (brightening, signifying disappearance or shrinkage of nevi) are displayed in green. The image can be enhanced even further by restricting red and green coloring to those pixels for which the differences between the first and second images exceed a specified threshold value.

This work was done by Robert H. Seiler of Caltech for **NASA's Jet Propulsion Laboratory.** *Further information is contained in a TSP [see page 1].*

In accordance with Public Law 96-517, the contractor has elected to retain title to this invention. Inquiries concerning rights for its commercial use should be addressed to

Technology Reporting Office
JPL
Mail Stop 122-116
4800 Oak Grove Drive
Pasadena, CA 91109
(818) 354-2240

Refer to NPO-19729, volume and number of this NASA Tech Briefs *issue, and the page number.*

National Aeronautics and
Space Administration

END

12-22-99